KiF1a-regulated neuronal infrastructures in sensory and prefrontal cortices essential for fear memory and anxiety

Jiayi Li, Bingchen Chen, Yun Zhang, Yang Xu, Lei Wang and Jin-Hui Wang*

College of Life Science, University of Chinese Academy of Sciences, Beijing China

Running title: associative memory neurons for psychological fear

Key words: fear memory, anxiety, associative memory cell, cerebral cortex, synapse and neuron

Word counter: Abstract, 186; Text, 7567.

***Correspondents author:**

Jin-Hui Wang, PhD and MD
Distinguished professor in neuroscience
University of Chinese Academy of Science
Beijing China 100049
wangjinhui@ucas.ac.cn

Abbreviations: AMN, associative memory neurons; mPFC, medial prefrontal cortex; VC, visual cortex; AC, auditory cortex; BS, battle sound; BI, battle image; Ob, observer; Con, control; KiF1a, kinesin family member-1a; RIP, resident/intruder paradigm; SIT, social interaction test, EPM, elevated-plus maze; LGB, lateral geniculate body; MGB, medial geniculate body; AP, anteroposterior; D-AP5, D-(-)-2-Amino-5-Phosphonopentanoic Acid; CNQX, 6-Cyano-7-Nitroquinoxaline-2,3-Dione.

Abstract (<200)

Stress in social activities induces fears. Cellular infrastructures and molecular profiles underlying fear memory to psychological stress remain elusive for designing therapeutic strategies. With making mice psychological trauma by watching fear scenes in a resident/intruder paradigm, we have studied the features of neuronal infrastructures in visual, auditory and medial prefrontal cortices correlated to this learned fear by the approaches of behavioral task, neural tracing, electrophysiology and molecular biology. This psychological trauma causes observational mice fear memory specific to resident mouse. This learned fear is associated with the formation of synapse interconnections among visual, auditory and medial prefrontal cortices and the strengthening of synapse interconnections among intramodal neurons. These cortical neurons receive new synapse innervations from their interconnected neurons alongside innate synapse innervations and become to encode the stress signals including battle image and battle sound inputted from these synapses. The *KiF1a* knockdown in the medial prefrontal cortex precludes the onsets of the neuronal infrastructures and the learned fear. KiF1a-mediated intracellular transportation in the medial prefrontal cortex is essential for the recruitment of associative memory neurons that encode fear scenes and anxiety.

48 **Highlight**

49 1) Psychological stress induces fears and interconnections among sensory and prefrontal cortices.

50 2) Associative memory neurons in these cortices are recruited to encode fear scenes and anxiety.

51 3) KiF1a-mediated transportation essential for these cellular infrastructures relevant to learned fear.

52

53 **Introduction**

54 The stress in social activities leads to the fear based on memory to stressful signals. The learned
55 fear endorses adaptative functions by activating defensive behaviors in the anticipation of dangerous
56 outcomes and minimizing the impact of threats (*1-3*). On the other hand, the learned fear by severe
57 persistent stress triggers posttraumatic stress disorder, obsessive-compulsive disorder and
58 generalized anxiety (*4-12*). These affective disorders in turn suppress the immune and cardiovascular
59 systems to cause secondary diseases (*13*). It is crucial to reveal the cellular and molecular mechanisms
60 underlying stress-induced fears and their impacts, which is the primary goal for the maintenance of
61 the moderate fear memory and the relief of the stress-induced pathological mood (*14, 15*). The
62 comprehensive diagram of neural circuits and molecular profiles for learned fear and its impacts is
63 expectedly figured to explore the adaptive and therapeutic strategies (*1, 14, 16-20*).

64 The learned fear may occur in the physical impairment by painful stresses and the psychological
65 trauma by observing and/or listening stressful episodes (*1-3, 21*). The neural correlates for the
66 learned fear based on fear memory have been studied by using the fear conditioning for rodents to
67 physically receive electrical shocks to their feet with bell ring or contexture (*8, 22-25*). The amygdala,
68 the nucleus accumbens and the medial prefrontal cortex are thought of as the critical regions in
69 relevance to the learned fear (*1, 25-54*). In another model of the body injury, the learned fear is
70 induced in the social stress by a resident/intruder paradigm (*7, 21, 55-62*). The stressful signals
71 including somatic injury pain and battle sound are detected by sensory receptors, inputted by afferent
72 nerves, encoded in sensory cortices and integrated through association cortices, the medial prefrontal
73 cortex and the amygdala, which are essential for fear responses (*21, 63, 64*). The studies by the gene
74 screening have identified many molecules relevant to the fear based on physical impairments,

including the activity-dependent genes, neuronal structure molecules and intracellular signal cascades (*7, 59-61, 65-69*). As the body injury is associated with the pain, cellular and molecular mechanisms underlying the pain and pain-relevant fear may be extensively overlapped and complicated (*20, 70*).

In comparison with the somatic pain-associated fear, the learned fear more commonly occurs in observing and listening stressful episodes that cause psychological traumas (*1-3, 71-73*). The neural locations and molecular profiles for the fear induced by the psychological trauma have been studied (*2, 7, 59, 60, 74-77*). In addition to the amygdala (*3, 73*), the auditory, visual and medial prefrontal cortices may be involved, since these cortical areas encode stressful signals and fear memories (*21, 41, 64, 78-84*). However, it is largely unknown what are the basic features of neuronal infrastructures in local cortical areas and the interconnections among cerebral cortices essential for the fear induced by the psychological trauma, how the memory trace to store psychological fear is constructed in the brain and how the cortical neurons are recruited to encode the stress signals and this type of the fear. Taken all of these questions, we aimed to examine how the observation and the listening of the stress episodes recruit the neuronal infrastructures correlated to the learned fear.

The strategies to address this question are given below. A C57 mouse as an observational subject (observer) was placed in face to a cage of resident/intruder paradigm, in which a resident CD1 mouse attacked an intruder C57 mouse, to induce the fear by the psychological trauma (*7, 55-58, 62, 85*). The formation of the learned fear was assessed by a social interaction test (SIT) and an elevated-plus maze test. The interconnections among the visual, auditory and medial prefrontal cortices were examined by the neural tracing with adeno-associated virus (AAV) vectors that carried the genes of encoding fluorescent proteins. Cellular infrastructures within these areas were investigated by the neural tracing to track axon interconnections and synapse formations among these cortical neurons

97 as well as by *in vivo* electrophysiological recordings in these cortical neurons to analyze their encoding
98 of the stressful signals including sounds and images recorded from the battle scenes. The recruitment
99 of associative memory neurons was ensured when new and innate synapse contacts were detected
100 convergently onto dendritic spines of axon-targeted neurons (*21, 86-88*) and when such cortical
101 neurons expressed the increased spike-encoding capability in response to fear signals (*86, 89, 90*). An
102 essential role of associative memory neurons, whose recruitment required motor protein kinesin for
103 the intracellular transportation, in the learned fear was examined by using RNAi specific to silence
104 kinesin family member-1a (*KiF1a*).
105
106 **Results**
107 The cellular infrastructure in medial prefrontal, visual and auditory cortices correlated to the fear
108 induced by psychological traumas is presented in this section. The fear in C57 juvenile mice was onset
109 after witnessing the attacks of a resident mouse to an intruder mouse in a resident/intruder paradigm,
110 in which stress signals included scare images and sounds in their battle. The synapse interconnections
111 were morphologically studied by neural tracing based on AAV vectors. The recruitment of associative
112 memory neurons was identified by both *in vivo* electrophysiological recording and neural tracing. The
113 associative memory neurons were surely recruited when cortical neurons receive convergent synapse
114 innervations from the axon boutons of new and innate pathways and became to encode stress signals.
115 The essential role of KiF1a in these processes was examined by shRNA specific for *KiF1a* knockdown.
116 **Psychological trauma by witnessing resident/intruder paradigm induces learned fear and anxiety**
117 In face to the cage of resident/intruder paradigm once a day for twelve days (a timeline in Figure
118 1A), observational mice (observers) were assessed by the social interaction test to examine the onset

of fear memory specific to this resident mouse and by the elevated-plus maze test to examine anxiety. Compared to control mice (left panel in Figure 1B), observers appear to stay away from this resident mouse placed in a small interaction box (right panel). The stay durations in an interaction zone, or the interaction time (seconds), in response to this resident mouse out of the total time (360 seconds) are 124.5 ±8.09 in observational mice (n=35) and 159.8±9 in controls (n=30, p=0.005, ANOVA, Figure 1C). In comparison with control mice (left panel in Figure 1D), the observers appear to stay away from the battle sound (right panel). The interaction time (seconds) in response to battle sounds is 100.3±5.25 in observers (n=36) and 123.9±6.61 in controls (n=27, p=0.007, ANOVA, Figure 1E). However, these control and observational mice do not show fear to the resident mouse and battle sounds before the experiments, and the observational mice appear not fear to mouse surrogates and the sound in their living environment after seeing resident/intruder paradigms (Figure S1). These results indicate that the mice of experiencing psychological traumas express fear memories specific to the resident mouse and battle sounds. Moreover, in comparison with control mice (left panel in Figure 1F), observational mice appear to avoid the open fields since they prefer to stay in the closed arms of the elevated-plus maze, EPM (right panel). The percentages of the stay time in the open arms over the total time on the EPM are 1.76±0.5% in observers (n= 16) and 7.87±1.6 % in controls (n=15, p=0.0008, ANOVA, Figure 1G), indicating that observational mice become more anxious. Therefore, psychological trauma leads to fear memory and anxiety-like behaviors.

In terms of cellular infrastructure underlying the learned fear in observational mice, we assumed that the auditory cortex was activated by battle sounds and the visual cortex was activated by battle scenes in a resident/intruder paradigms simultaneously. Based on the principle of coactivity together and interconnection together that recruits associative memory neurons **(*14, 90, 91*)**, we further

assumed that the stress signal instigated the new synapse interconnections among auditory, visual and prefrontal cortices to recruit these cortical neurons to be associative memory neurons that specifically encode stressful signals and fears.

Psychological trauma recruits new synapses and associative memory neurons to encode fear signals

The synapse interconnections between auditory and visual cortices and the synapse innervations from such cortices toward the medial prefrontal cortex were examined by the neural tracing with AAV vectors. 0.3 μl AAV-CMV-tdTomato and 0.3 μl AAV-CMV-BFP were microinjected in the visual cortex and the auditory cortex, respectively (Figure 2A). Three days after AAV injection, these mice observed the attack of CD1 resident mouse to C57 intruder mouse in resident/intruder paradigm to experience psychological trauma or stayed in a witness cage without C57 intruder mouse once a day for twelve days. The brain slices including visual, auditory and medial prefrontal cortices from two groups were scanned under a confocal microscope. In the visual cortex, the contacts of BFP-labelled axon boutons on YFP-labelled dendritic spines were thought of as the synapses made by those axons crossmodally projected from the auditory cortex, and the contacts of RFP-labelled axon boutons on YFP-labelled dendritic spines were the synapses made by those axons among intramodal visual cortical neurons. In the auditory cortex, the contacts of RFP-labelled axonal boutons on YFP-labelled dendritic spines were the synapses made by the axons crossmodally from the visual cortex, and the contacts of BFP-labelled axon boutons on YFP-labelled dendritic spines were the intramodal synapses. In the medial prefrontal cortex, the contacts of BFP- and RFP-labelled axons on YFP-labelled dendritic spines were convergent synapse innervations made by the axons crossmodally from the auditory cortex and the visual cortex.

When the neurons in visual, auditory and medial frontal cortices receive two sources of synapse inputs, these cortical neurons are theoretically able to encode battle images and battle sounds in the

163 resident/intruder paradigm, i.e., they are recruited to be associative memory neurons in morphology
164 (*14, 21, 64*). Moreover, *in vivo* electrophysiological recordings in these cortices were conducted to
165 examine whether these cortical neurons become able to encode battle sounds and images. Spike
166 frequencies were an index of neuron-activity strength. The evoked spikes on the background of
167 spontaneous spikes were analyzed. Normalized spike frequency in response to one of stressful signals
168 was calculated to be the ratio of the frequency of evoked spikes to the frequency of spontaneous
169 spikes in 30 seconds before stimuli. If these ratios reached 1.5 or above, the recorded neurons were
170 deemed as the responses to these signals. The neurons responded to one of two signals were called as
171 active neurons. Auditory, visual and medial prefrontal cortical neurons in response to battle images
172 and battle sound were presumably associative memory neurons in function, similar to previous
173 studies (*14, 21, 64, 86, 90, 91*).

174 ***New synapses and associative memory neurons in the visual cortex*:** BFP-labelled axon boutons
175 from auditory cortex to the visual cortex and their synapse contacts on visual cortical neurons appear
176 more in observers with the fear memory (bottom panel in Figure 2B) than controls (top panel). Axon
177 boutons per mm^3 are $7.44x10^5 \pm 0.73x10^5$ in observers (n=34 cubes from 5 mice) and $5.34x10^5 \pm 0.74x$
178 10^5 in control group (n=31 cubes from 5 mice, $p<0.05$, ANOVA, Figure 2C). Synapse contacts per 100
179 µm dendrite on visual cortical neurons are 2.58±0.3 in observers (n=28 dendrites from 5 mice) and
180 1.17±0.2 in controls (n=19 dendrites from 5 mice, p=0.0015, ANOVA, Figure 2D). Furthermore, to the
181 intramodal axon boutons and synapses in the visual cortex, the RFP- labelled axon boutons and their
182 synapse contacts appear more in observers with fear memory (bottom panel in Figure 2E) than in
183 controls (top panel). Axon boutons per mm^3 are $7.57x10^5 \pm 1.41x10^5$ in observers (n=14 cubes from 4
184 mice) and $2.45x10^5 \pm 0.87x10^5$ in controls (n=26 cubes from 4 mice, p=0.0024, ANOVA, Figure 2F).

185 Synapse contacts per 100 μm dendrite on visual cortical neurons are 2.48±0.4 in observers (n=12
186 dendrites from 4 mice) and 1.03 ±0.26 in controls (n=13 dendrites from 4 mice, p=0.0048, ANOVA,
187 Figure 2G). These data indicate that the synapse connections from the auditory cortex to the visual
188 cortex and the synapse interconnections among visual cortical neurons are formed and increased in
189 observational mice with the fear memory induced by psychological traumas. The formation of new
190 synapses is also supported by the upregulation of dendritic spines on visual cortical neurons from
191 observational mice (Figure S5).

192 In the recording of unitary discharges at visual cortical neurons, battle sound and battle image in
193 30 seconds were given sequentially to observational mice with fear memory and control mice (Figure
194 2H). Some visual cortical neurons appear responding to both battle sound and image in observational
195 mouse with fear memory (red trace in Figure 2I), but not control mouse (blue trace). The percentages
196 of associative memory neurons in total active neurons were 38.89 % in observers (n=21/54 from 19
197 mice) and 14.89% in controls (n=7/47 from 15 mice; χ^2=7.22, p=0.007, Chi-square test, Figure 2J). Such
198 visual cortical neurons in observers do not respond to sounds in their living environments (Figure S2).
199 This result indicates that the synapse innervations to visual cortical neurons from the auditory cortex
200 recruit them to encode battle sounds and battle images, or associative memory neurons, for the joint
201 storage of fear signals. This indication is granted by a result that the number of visual cortical neurons
202 in response to battle sounds is more in observers than in controls (χ^2=4.55, p=0.033, Figure 2K). In
203 addition, normalized spike frequencies at active visual cortical neurons in response to battle sounds
204 are 2.62 ±0.20 in observers (n=31 cells from 19 mice) and 1.96±0.15 in control (n=17 cells from 15
205 mice, p=0.026, ANOVA, Figure 2L), indicating that the synapse innervations from the auditory cortex
206 (Figure 2B-D) enhance the excitatory activity of visual cortical neurons. Normalized spike frequencies

207 at active visual cortical neurons in response to battle images are 2.57±0.22 in observers (n=44 cells
208 from 19 mice) and 1.87± 0.08 in controls (n=37 cells from 15 mice, p=0.006, ANOVA, Figure 2M),
209 indicating that the synapse innervations raised within intramodal visual cortex (Figure 2E-G) enhance
210 the excitatory activity of visual cortical neurons.

211 ***New synapses and associative memory neurons in auditory cortex*:** RFP-labelled axon boutons
212 from the visual cortex to the auditory cortex and their synapse contacts appear more in observational
213 mice with fear memory (bottom panel in Figure 3A) than controls (top panel). Axon boutons per mm^3
214 are $4.76x10^5$± $0.66x10^5$ in observer (n=35 cubes from 5 mice) and $2.54x10^5$±$0.27\ x10^5$ in control (n=25
215 cubes from 5 mice, p=0.008, ANOVA, Figure 3B). Synapse contacts per 100 µm dendrite on auditory
216 cortical neurons are 1.68±0.18 in observers (n=35 dendrites from 5 mice) and 0.83±0.18 in controls
217 (n=16 dendrites from 5 mice, p=0.0049, ANOVA, Figure 3C). Furthermore, to intramodal axon boutons
218 and synapses in the auditory cortex, BFP-labelled synapse contacts appear more in observers with
219 fear memory (bottom panel in Figure 3D) than in controls (top panel). Axon boutons per mm^3 are
220 $3.77x10^6$±$0.59x10^6$ in observers (n=26 cubes from 5 mice) and $3.26x10^6$±$0.35x10^6$ in controls (n=43
221 cubes from 6 mice, p=0.43, ANOVA, Figure 3E). Synapse contacts per 100 µm dendrite on auditory
222 cortical neurons are 2.61±0.33 in observers (n=24 dendrites from 9 mice) and 1.46±0.23 in controls
223 (n=31 dendrites from 5 mice, p=0.0049, ANOVA, Figure 3F). Thus, the synapse connections from the
224 visual cortex to the auditory cortex as well as the synapse interconnections among auditory cortical
225 neurons are formed and increased in observational mice with fear memory induced by psychological
226 trauma. The formation of new synapses is also granted by the change of dendritic spines on auditory
227 cortical neurons from observational mice (Figure S5).

228 The *in vivo* electrophysiological recordings in the auditory cortex were used to examine whether

229 auditory cortical neurons become able to encode battle sound and battle image (Figure 3G). Auditory
230 cortical neurons respond to both battle sounds and images in observational mouse with fear memory
231 (red trace in Figure 3H), but not in control mouse (blue trace). The percentages of associative memory
232 neurons in total active neurons were 45% in observers (n=27/60 from 19 mice) and 22% in controls
233 (n=9/41 from 14 mice; χ^2= 5.641, p=0.018, Chi- square test, Figure 3I). These auditory cortical neurons
234 in observers do not respond to flower images (Figure S2). This result indicates that the synapse inputs
235 to auditory cortical neurons from the visual cortex recruit them to encode battle sounds and images,
236 or associative memory neurons, for the joint storage of fear signals. This indication is supported by the
237 result that the number of auditory cortical neurons in response to battle images is more in observers
238 than in controls (χ^2=10.35, p=0.001, Figure 3J). Furthermore, normalized spike frequencies at active
239 auditory cortical neurons in response to battle sounds are 2.59±0.17 in observers (n=47 cells from 15
240 mice) and 2.04±0.11 in controls (n=36 cells from 14 mice, p=0.01, ANOVA, Figure 3K), indicating that
241 the synapse innervations raised in the intramodal auditory cortex (Figure 3D) enhance the excitatory
242 activity of auditory cortical neurons. However, normalized spike frequencies at active auditory cortical
243 neurons in response to battle images are 2.36±0.15 in observers (n=40 cells from 15 mice) and
244 2.4±0.37 in controls (blue bar, n=14 cells from 15 mice, p=0.92, ANOVA, Figure 3K), implying that the
245 synapse innervations increased from the cross-modal visual cortex (Figure 3A-C) are not sufficient to
246 enhance the excitatory activity of auditory cortical neurons.

247 ***New synapses and associative memory neurons in the medial prefrontal cortex*:** As the medial
248 prefrontal cortex locates at the downstream of sensory cortices in neuronal signal flows **(*92:Yeterian,***
249 ***2012 #40153*)** and prefrontal cortical neurons can be recruited as associative memory cells to encode
250 physiological signals **(*63, 93, 94*)**, these medial prefrontal cortical neurons may be recruited as

251 associative memory neurons to encode the fear signals in psychological traumas based on receiving
252 convergent synapse innervations from visual and auditory cortices.

253 To study axon boutons and their synapse contacts in the medial prefrontal cortex crossmodally
254 from visual and auditory cortices, we microinjected 0.3 µl AAV-CMV-tdTomato in the visual cortex and
255 0.3 µl AAV-CMV-BFP in the auditory cortex (top panel in Figure 4A). RFP-labelled axon boutons, BFP-
256 labelled axon boutons and synapse contacts made by these axon inputs appear more in the medial
257 prefrontal cortex in observational mice with fear memory (bottom panel in Figure 4B) than in controls
258 (top and middle panels). Axon boutons per mm^3 in the medial prefrontal cortex are $1.82x10^6 \pm 0.4x10^6$
259 in observers (n=27 cubes from 5 mice) and $0.63x10^6 \pm 0.14x10^6$ in controls (n=36 cubes from 5 mice,
260 p=0.003, ANOVA, Figure 4C). Synapse contacts per 100 µm dendrite on medial prefrontal cortical
261 neurons are 2.18±0.2 in observers (n=31 dendrites from 5 mice) and 0.81±0.16 in controls (n=22
262 dendrites from 5 mice, p<0.0001, ANOVA, Figure 4D). Moreover, to examine intramodal axon boutons
263 and their synapse contacts in the medial prefrontal cortex, we microinjected 0.3 µl AAV-CMV-EGFP in
264 this area (bottom panel in Figure 4A). GFP-labelled intramodal axon boutons and the synapse contacts
265 appear more in observers with fear memory (bottom panel in Figure 4E) than in controls (top panel).
266 Axon boutons per mm^3 are $1.07x10^7 \pm 0.39x10^7$ in observers (n=12 cubes from 5 mice) and $0.27x10^7 \pm$
267 $0.1x10^7$ in controls (n=16 cubes from 5 mice, p=0.035, ANOVA, Figure 4F). Synapse contacts per 100
268 µm dendrite on medial prefrontal cortical neurons are 4.42±0.43 in observers (n=10 dendrites from 4
269 mice) and 2.99±0.45 in controls (n=9 dendrites from 4 mice, p=0.036, ANOVA, Figure 4G). Therefore,
270 the convergent synapse innervations on medial prefrontal cortical neurons from visual and auditory
271 cortices and the synapse interconnections among medial prefrontal cortical neurons are formed and
272 increased in observational mice with fears.

The *in vivo* electrophysiological recordings in the medial prefrontal cortex were used to examine whether medial prefrontal cortical neurons become able to encode stressful signals (Figure 4H). Some medial prefrontal cortical neurons respond to battle sounds and images in observational mouse with fear memory (red trace in Figure 4I), but not control one (blue trace). The percentages of associative memory neurons in the total neurons were 19.77 % in observers (n=17/86 from 10 mice) and 3.17% in controls (n=2/63 from 7 mice; χ^2= 9.0, p=0.003, Chi-square test, Figure 4J). Medial prefrontal cortical neurons in observers do not respond to the environmental sound and flower image (Figure S2). These data indicate that synapse innervations on medial prefrontal cortical neurons from visual and auditory cortices recruit them to encode battle sound and battle image, or associative memory neuron, for the learned fear induced by psychological traumas. This indication is granted by a result that the number of medial prefrontal cortical neurons in response to battle image or battle sound is more in observers than controls (χ^2=12.96, p=0.0003, Figure 4K). Furthermore, normalized spike frequencies at medial prefrontal cortical neurons in response to battle sound are 1.61±0.14 in observers (n=86 cells from 10 mice) and 0.99±0.08 in controls (n=63 cells from 7 mice, p=0.0005, ANOVA, Figure 4L). Normalized spike frequencies at medial prefrontal cortical neurons in response to battle images are 1.74±0.13 in observers (n=86 cells from 10 mice) and 1.22±0.11 in controls (n=63 cells from 7 mice, p=0.0035, ANOVA, Figure 4M). These data indicate that the synapse innervations on medial prefrontal cortical neurons increased from cross-modal visual and auditory cortices (Figure 4B-D) and among intramodal neurons (Figure 4E-G) strengthen the excitatory activity of medial prefrontal cortical neurons.

Both morphological and electrophysiological data validate that psychological traumas recruit the associative memory neurons in visual, auditory and medial prefrontal cortices. The formation of new synapse innervations in these cortices crossmodally from their interconnected areas in the mice with

295 fear memory recruits cortical neurons to be associative memory neurons that encode fear signals. The
296 synapse innervations from cross-modal cortical neurons as well as the synapse interconnection among
297 intramodal neurons strengthen the spike-encoding of associative memory neurons and active cortical
298 neurons.

299 **Kinesin family member-1A is required for recruiting associative memory neurons to encode fears**

300 In terms of the mechanism underlying the recruitment of associative memory neurons to encode
301 fear memory, the molecules related to the axon growth and transportation for the interconnection of
302 visual, auditory and medial prefrontal cortices are likely involved. Kinesins are motor proteins for the
303 intracellular transportation of vesicles in axons and receptors in dendrites as well as the function of
304 synapses (*95-106*), which are relevant to the learning and memory (*107, 108*). Kinesins are also highly
305 expressed in the medial prefrontal cortex of observational mice (Figure S3). We hypothesized that
306 kinesins might be required for the elongation of axons, the enlargement of dendritic spines and the
307 formation of new synapses to recruit associative memory neurons to encode fears. The knockdown of
308 kinesin family member-1a (KiF1a) in the medial prefrontal cortex was conducted to examine the
309 requirement of KiF1a for these processes. A rationale for using *KiF1a* knockdown to suppress the
310 recruitment of associative memory cells is based on the axon projection for their recruitment (*21, 64,*
311 *86, 88 Wang, 2019 #38551, 90*). AAV-carried RNAi specific to *KiF1a* (AAV-U6-shKiF1a-GFP) was
312 injected in medial prefrontal cortices of observational mice five days before facing to a
313 resident/intruder paradigm (bottom panel in Figure 5A). This shRNA has been proven to reduce KiF1a
314 expression in the medial prefrontal cortex (Figure S3). shRNA scramble control was injected in
315 another group of observational mice. The experiments in *KiF1a* knockdown (*KiF1a*-KD) were
316 conducted with behavioral tasks, neural tracing and electrophysiology *in vivo* used in Figures 1-4. The

317 essential roles of KiF1a in the onset of fear memory, the formation of new synapse innervations and
318 the recruitment of associative memory cells would be ensured if these processes were lowered in
319 observational mice with *KiF1a* knockdown.

320 AAV-CMV-tdTomato and AAV-CMV-BFP were microinjected in the visual cortex and the auditory
321 cortex, respectively, when AAV-U6-shKiF1a-GFP was injected in the medial prefrontal cortex (Figure
322 5A). RFP-labelled axon boutons from the visual cortex, BFP-labelled axon boutons from the auditory
323 cortex and such axon-made synapse contacts on dendritic spines of medial prefrontal cortical neurons
324 (yellow) appear lower in observational mice with *KiF1a*-KD (bottom panel in Figure 5B) than scramble
325 control mice (top panel). Axon boutons per mm^3 in the medial prefrontal cortex are $3.48x10^5$±0.65x
326 10^5 in *KiF1a*-KD group (n=51 cubes from 5 mice) and $9.52x10^5$± $0.76x10^5$ in scramble controls (n=69
327 cubes from 5 mice, $p<0.0001$, ANOVA, Figure 5C). Synapse contacts per 100 µm dendrite on medial
328 prefrontal cortical neurons are 0.85±0.15 in *KiF1a*-KD (n=36 dendrites from 5 mice) and 2.22±0.21 in
329 scrambles (n=62 dendrites from 5 mice, $p<0.0001$, ANOVA, Figure 5D). Moreover, intramodal axon
330 boutons and their synapse contacts in the medial prefrontal cortex were examined by GFP-mediated
331 tracing (AAV-U6-shKiF1a-GFP, bottom panel in Figure 5A). GFP-labelled intramodal axon boutons and
332 their synapse contacts appear lower in observers with *KiF1a*-KD (bottom panel in Figure 5E) than in
333 scrambles (top panel). Axon boutons per mm^3 are $9.25x10^5$±$1.16x10^5$ in *KiF1a*-KD (n=46 cubes of 5
334 mice) and $17.74x10^5$±$2.49x10^5$ in scrambles (n=50 cubes from 9 mice, $p<0.01$, ANOVA, Figure 5F).
335 Synapse contacts per 100 µm dendrite on medial prefrontal cortical neurons are 2.42±0.17 in *KiF1a*-
336 KD (n=38 dendrites from 5 mice) and 3.68±0.32 in scrambles (n=19 dendrites from 5 mice, $p=0.0003$,
337 ANOVA, Figure 5G). KiF1a is required for the formation of new cross-modal and intramodal synapse
338 innervations and for the recruitment of associative memory neurons in the medial prefrontal cortex

339 induced by psychological traumas.

340 The *in vivo* electrophysiological recordings in the medial prefrontal cortex were done to examine
341 the functional effectiveness of KiF1a on the recruitment of associative memory neurons in the medial
342 prefrontal cortex (Figure 5H). Medial prefrontal cortical neurons respond to battle sound and images
343 in scramble control mouse (blue trace in Figure 5I), but not observer with *KiF1a*-KD (red trace). The
344 percentages of associative memory neurons in all neurons were 4.08% in *KiF1a*-KD (n=2/49 from 7
345 mice) and 25.37% in scramble control (n=17/67 from 7 mice; χ^2= 9.37, p=0.002, Chi-square test, Figure
346 5J). The downregulation of synapse innervations on medial prefrontal cortical neurons from visual and
347 auditory cortices precludes them to encode battle sound and battle images in fear memories induced
348 by psychological traumas. This indication is granted by the data that the number of medial prefrontal
349 cortical neurons in response to battle images or battle sounds is more in scrambles than in *KiF1a*-KD
350 (χ^2=7.41, p=0.007, Figure 5K). Moreover, normalized spike frequencies at medial prefrontal cortical
351 neurons in response to battle sound are 1.05±0.13 in *KiF1a*-KD (n=49 cells from 7 mice) and 1.71±0.17
352 in scrambles (n=67 cells from 7 mice, p=0.0047 ANOVA, Figure 5L). Normalized spike frequencies at
353 medial prefrontal cortical neurons in response to battle images are 0.96±0.12 in *KiF1a*-KD (n=49 cells
354 from 7 mice) and 1.75±0.19 in scrambles (n=67 cells from 7 mice, p=0.002, ANOVA, Figure 5M). Thus,
355 the downregulation of synapse innervations from cross-modal and intramodal cortices to the medial
356 prefrontal cortical neurons that encode battle sound and battle images for fear memory weakens the
357 excitatory activity of medial prefrontal cortical neurons.

358 In the experiment of behavior tasks, the observational mice with KiF1a-KD appear not to avoid
359 the resident mouse (right panel in Figure 6A), compared with scramble control mice (left panel). The
360 interaction time (seconds) in response to a resident mouse is 125.6±8.3 in *KiF1a*-KD mice (n=16) and

361 88.96±8.53 in scrambles (n=14; p=0.0047, ANOVA, Figure 6B). Furthermore, the interaction time in
362 response to battle sound appears lower in scramble controls (left panel in Figure 6C) than *KiF1a*-KD
363 mice (right panel). The interaction time (second) in response to battle sound is 121.1±8.62 in
364 *KiF1a*-KD mice (n=17) and 88.26±5.52 in scramble mice (n=16, p<0.01, ANOVA, Figure 6D). It is
365 noteworthy that the mice with injections of AAV-U6-sh*KiF1a*-GFP and scramble controls in medial
366 prefrontal cortices do not show fear to CD1 resident mouse, battle sound, housing environment sound
367 and mouse surrogate before the experiments as well as not fear to housing environment sound and
368 mouse surrogates after the psychological trauma (Figure S4). Therefore, *KiF1a* knockdown in the
369 medial prefrontal cortices of observational mice precludes the retrieval of fear memories to resident
370 mice and battle sounds.

371 The influence of *KiF1a* knockdown on anxiety-like behaviors of observational mice was examined
372 by using elevated-plus maze (EPM). Stay time on the plate of open arms in the EPM appears longer in
373 the observational mice with *KiF1a*-KD (right panel in Figure 6E) than scramble control mice (left panel).
374 The ratios of the stay time on the plate of the open arms to the total time in the EPM are 8.22±1.61%
375 in *KiF1a*-KD mice (n=9) and 0.96±0.31% in scramble control mice (n=9, p=0.0004, ANOVA, Figure 6F).
376 The *KiF1a* knockdown in medial prefrontal cortices of observational mice precludes their anxiety-like
377 behaviors induced by psychological traumas. These data indicate that KiF1a in the medial prefrontal
378 cortex plays an essential role in stress-induced fear memory and anxiety.

379 **Associative memory neurons in the medial prefrontal cortex are secondary in nature**

380 Psychological traumas recruit associative memory neurons that encode stressful signals in visual,
381 auditory and medial prefrontal cortices. As the medial prefrontal cortex anatomically and functionally
382 locates at the downstream of visual and auditory cortices, the associative memory neurons in sensory

383 cortices might be primary, and the associative memory neurons in the medial prefrontal cortex might
384 be secondary (*63, 93, 94*). The assumption can be proven if the encoding of stress signals at
385 associative memory neurons in the medial prefrontal cortex is prevented by downregulating the
386 recruitment of associative memory neurons in sensory cortices as well as blocked by inhibiting the
387 activity of sensory cortical neurons. The prevention of recruiting the associative memory neurons in
388 visual and auditory cortices was conducted by the *KiF1a* knockdown in these areas. The activity
389 blockage of visual and auditory cortical neurons was conducted by CNQX and D-AP5, the antagonists
390 of inotropic glutamate receptors, in these areas.

391 The KiF1a knockdown in visual and auditory cortices of observational mice (Figure 7A) appears to
392 prevent the responses of medial prefrontal cortical neurons to battle sounds and battle images (red
393 trace in Figure 7B), in comparison with scramble controls (blue trace). The percentages of associative
394 memory neurons in total neurons were 7.46% in KiF1a-KD group (n=5/67 from 4 mice) and 24.1% in
395 scramble group (n=13/54 from 4 mice; χ^2= 6.52, p= 0.01, Chi-square test, Figure 7C). The percentages
396 of active neurons in total neurons were 40.3% in KiF1a-KD group (n=27/67 from 4 mice) and 62.96% in
397 scramble controls (n= 34/54 from 4 mice; χ^2= 6.14, p=0.01, Chi-square test, Figure 7D). Moreover, the
398 blockages of ionotropic glutamate receptors in the visual and auditory cortices of observational mice
399 by 10 μM CNQX and 40 μM D-AP5 (Figure 7E) appear to attenuate the responses of medial prefrontal
400 cortical neurons to battle sounds and images (Figure 7F). The ratios of normalized spike frequencies in
401 responses to battle sounds (Figure 7G) and battle images (Figure 7H) are attenuated to less 1.5. These
402 suppressed responses of associative memory neurons to stress signals in the medial prefrontal cortex
403 by downregulating the activities of visual and auditory cortices indicate that the associative memory
404 neurons in sensory cortices are primary and the associative memory neurons in the medial prefrontal

405 cortex are secondary in nature.

406

407 **Discussion**

408 The psychological trauma by watching a resident/intruder paradigm causes the fear memory
409 specific to stressful scenes and anxiety-like behaviors (Figure 1). In the mice with this learned fear,
410 the synapse interconnections between visual and auditory cortices and their convergent synapses
411 on medial prefrontal cortical neurons are newly formed and functionally active. Some neurons in
412 these cortical areas become able to encode the stressful signals including battle sound and battle
413 images (Figures 2-4). That is, psychological trauma recruits associative memory neurons in neural
414 pathways from the visual and auditory cortices to the medial prefrontal cortex (Figures 2-4) that
415 encode fear signal. The recruitment of associative memory neurons and the onset of learned fear
416 are precluded by KiF1a knockdown, one of motor proteins (Figures 5-6). Therefore, psychological
417 trauma recruits visual, auditory and medial prefrontal cortical neurons as the associative memory
418 neurons that encode the learned fear by KiF1a-mediated transportation of intracellular molecules
419 and organelles.

420 In terms of the mechanisms for the recruitment of associative memory neurons in auditory,
421 visual and medial prefrontal cortices as well as the onset of learned fear, our interpretations are
422 given below. The stress signals in the battle scenes of resident/intruder paradigm were dissected
423 and sensed by the visual and auditory sensory systems, which activate visual and auditory cortical
424 neurons. Based on the principle of coactivity together and interconnection together (*14, 90, 91*),
425 the simultaneously intensive activities of these cortical neurons instigate the biophysical and
426 biochemical cascades from higher frequency action potentials to epigenetic events (*14, 86-89*), which

427 in turn trigger the axon elongation (*14, 86, 88*) and enhance KiF1a-mediated intracellular
428 transportations (*95-101, 103*). These neural events facilitate the projection of elongated axons to their
429 active target areas as well as the transportation of presynaptic vesicles and construction molecules for
430 axon innervations to their target neurons (*95, 97, 100*)(Figures 2-4). The biophysical and biochemical
431 cascades in coactive postsynaptic neurons may induce the expansion of dendritic arbors, the
432 transportation of dendritic molecules (*103-106, 109, 110*) and the increase of dendritic spines (*21*)
433 (Figure S5). The upregulations of presynaptic axonal arbors and postsynaptic dendritic spines
434 coordinately work for the formation of new synapses. When presynaptic boutons and postsynaptic
435 spines contact, these new synapses need be anchored and fixed by synapse-linkage proteins, e.g.,
436 neuroligins and neurexin (*21, 64, 111-114*). Whether the expansion of dendrites and their spines
437 requires a KiF1a-mediated intracellular transportation about postsynaptic receptors and
438 synapse-building molecules remains to be examined. New axon projection, spine increase and
439 synapse formation endorse cortical neurons to interconnect synaptically along with receiving their
440 previously formed synapses, such that the associative memory neurons are recruited in neural
441 pathways from sensory cortices to the medial prefrontal cortex that encode fear memory and anxiety.

442 Our data reveal that the psychological trauma induces the fear memory specific to stress signals
443 in battle scenes and the anxiety-like behaviors by the recruitment of associative memory neurons in
444 memory traces based on the KiF1a-mediated intracellular transportation. The downregulation of
445 KiF1a expression in the medial prefrontal cortex relieves fear memory and anxiety-like behaviors,
446 such that KiF1a-mediated process may be one of the targets for the relief of severe and persistent
447 fear memory that may cause posttraumatic stress disorder, obsessive-compulsive disorder and
448 generalized anxiety (*4-12*). On the other hand, the learned fear may endorse the adaptative functions

449 by activating the defensive behaviors in the anticipation of dangerous outcomes and minimizing the
450 impact of threats (*1-3*). It is crucial to further study the quantitative knockdown of KiF1a in order to
451 find its borderline level for maintaining moderate fear memory versus for relieving pathological
452 moods induced by severe and persistent stress (*14, 15*).

453 The previous studies about the neural correlates for the learned fear or fear memory have been
454 conducted by using the fear conditioning for rodents to physically receive the electrical shocks to their
455 feet with bell rings or contexture (*8, 22-25*). As the current of electrical shocks may spread to the
456 entire body and activate all of the neurons in the nervous system (*14, 21, 58, 62, 64, 85*), the
457 coactivity of these neurons may cause the neural circuits in relevance to this electrical stress to be
458 broad interconnections. The learned fear is also studied by the body impairment in resident/intruder
459 paradigm (*7, 21, 55-60, 62*). The stressful signals including somatic injury pain and battle sounds are
460 detected by multiple sensory systems, encoded in the sensory cortices and integrated in the medial
461 prefrontal cortex and amygdala (*21, 63, 64*). As the body injuries are accompanied by pain, the
462 cellular and molecular mechanisms for the pain and the pain-relevant fear are overlapped (*20, 70*).
463 The neuronal circuits correlated to these stressful paradigms may not specifically represent the
464 features of cellular infrastructure in the learned fear. On the other hand, compared with somatic
465 pain-associated fear, the learned fear more commonly occurs in observing and listening the stress
466 episodes that cause psychological trauma (*1-3, 71-73*). Thus, the neural allocations and molecular
467 profiles for the fear induced by the psychological trauma should be studied (*2, 7, 74-77*). In addition
468 to the amygdala (*3, 73*), the visual, auditory and medial prefrontal cortices are likely involved, since
469 these cortices encode the stressful signals and fear memories (*21, 41, 64, 78-84*). In present study, we
470 have looked through the basic features of neuronal infrastructures in visual, auditory and medial

471 prefrontal cortices that are correlated to the fear induced by psychological trauma. In those mice with
472 the fear memory specific to the stressful scenes induced by the psychological trauma, the synapse
473 interconnections emerge among visual, auditory and medial prefrontal cortices as well as among
474 intramodal neurons. Some neurons in these cortices become able to encode the stressful signals.
475 All of these changes for the recruitment of associative memory neurons rely on KiF1a-mediated
476 intracellular transportation. Our data provide new insights for cellular and molecular mechanisms
477 underlying fear memory and anxiety.

478 The auditory cortex and the visual cortex presumably encode associative learning and memory
479 (*80, 84, 115-124*). The medial prefrontal cortex is correlated to the integration of the associative
480 memories including cognition-relevant memory and fear memory (*37, 50, 63, 78, 125-130*). The
481 neural circuits among these cortices, the cellular infrastructure and the mechanisms correlated to the
482 associative memory remain unclear. Our results indicate that the emergence of the fear memory
483 induced by psychological trauma is coupled with the KiF1a-mediated synapse interconnections among
484 these cortical areas and among their intramodal neurons, which are recruited as the associative
485 memory neurons to encode the stressful signals and learned fear. These associative memory neurons
486 to encode psychological processes in pathology functionally differ from those associative memory
487 neurons to encode the physiological signals for the cognitive activity (*86, 87, 90, 91, 131, 132*). The
488 molecular profiles for the recruitment of associative memory neurons that encode the physiological
489 signals and the molecular profiles for the recruitment of associative memory neurons to encode
490 pathological signals should be addressed in order to selectively manipulate these two groups of
491 associative memory neurons, which may benefit to maintain physiological memories and expunge
492 pathological memories. It is noteworthy that the molecular markers for engrams have been thought

493 of immediate early genes (*133-135*). However, these genes are nonspecific in those overly active
494 neurons, e.g., excitotoxicity cells, epileptic cells and pain-relevant cells (*136-142*). A partial
495 colocalization of associative memory neurons and *cFos*-labelled neurons indicates that such two
496 populations are not identical, or not mutually represented (*64*).

497 In summary, the psychological traumas by the formation of new synapse interconnections among
498 cross-modal visual, auditory and medial prefrontal cortices and among the intramodal neurons recruit
499 them to be associative memory neurons that encode stress signals and fear. The associative memory
500 neurons of encoding psychological behaviors are primary in visual and auditory cortices and secondary
501 in the medial prefrontal cortex. The stress-induced psychological activities and cellular infrastructure
502 changes are based upon KiF1a-mediated intracellular transportation. The coactivity of cortical neurons
503 induced by the psychological trauma towards the KiF1a-mediated processes and their featured cellular
504 infrastructures are illustrated in Figure 8.

505

506 **Materials and Methods**

507 **Studies approved in mice and animal's feeding:** Experiments were conducted in accordance with
508 the guidelines and regulations by the Administration Office of Laboratory Animals in Beijing China. All
509 experimental protocols were approved by the Institutional Animal Care and Use Committee in Beijing
510 China (B10831).

511 Two species of mice have been utilized in our experiments. C57BL/6JThy1-YFP mice (Jackson Lab,
512 JAX stock #003782, USA) were used, whose glutamatergic neurons in the cerebral brain were labelled
513 genetically by the yellow fluorescent protein (YFP) (*143, 144*). These C57BL/6JThy1-YFP male and
514 female mice were randomly divided into control group and observational group in face to the

515 resident/intruder paradigm (RIP). This observational group also included the two subgroups in faces to
516 RIP plus *KiF1a* knockdown and to RIP plus shRNA scramble control. CD1 mice above three months
517 with more aggression were used as resident mice. The well-developed C57 mice on postnatal days
518 (PND) 21 were selected and placed into an observation cage neighboring to the cage used for
519 resident/intruder paradigm. These two cages were separated by a transparent and punctured wall
520 (Figure 1A). When C57 mice were faced to a cage including resident mouse and intruder mouse, they
521 were observational mice (observers). When C57 mice were faced to a cage without intruder mice,
522 they were control mice. Before facing to a resident/intruder paradigm, observational mice and control
523 mice were examined by the social interaction test (SIT) to identify their fear memory specific to a CD1
524 mouse and by the elevated-plus maze (EPM) test to assess their anxious state (*7, 21*). The two groups
525 of mice show no statistical differences in these tests (Figure S1). These mice were accommodated in
526 the specific pathogen-free facility with the circadian of twelve hours for night and day plus self-help
527 feeding. The face to resident/intruder paradigms and the behavioral tests were conducted during the
528 daytime of this circadian.

529 **Behavioral study**: C57 mice were fetched to the laboratory to accommodate experimenters and
530 the training apparatus for two days and were randomly assigned into observational group and control
531 group. The resident/intruder paradigm is introduced by the following references (*7, 21, 55-58, 62*) and
532 Figure 1A. In the meantime of doing resident/intruder paradigm, one observational mouse was placed
533 in a neighboring cage with the transparent and perforated glass- plate to separate two cages (Figure
534 1A). The times, duration and period for observational mice facing to the attacks of a CD1 mouse to an
535 intruder mouse in a resident/intruder paradigm were set as once a day for 30-90 seconds and twelve
536 days in total (Figure 1A). The protocol of this psychological trauma was also modified in the stressful

537 intensity daily during twelve-day training period, in order to reduce the habituation of observational
538 mice to the stresses. The battle image in the attacks of CD1 mouse to C57 mouse in resident/intruder
539 paradigm and the motional tracks of observational and control mice in the social interaction box were
540 recorded by the video camera located above these open fields. The battle sound was recorded by a
541 tiny audio recorder. That is, the complete procedure in the attacks of CD1 mice to C57 mice and their
542 battle sound were recorded at the same time for the subsequent uses in the social interaction test
543 and electrophysiological studies. The observational mice were sent back to their home-cage and
544 housed individually. In control procedures, C57 mice were placed in the cage neighboring the cage for
545 resident/intruder paradigm in the absence of intruder mouse.
546 The social interaction test was conducted in open field box (50 cm x 50 cm) that included small
547 transparent and perforated box (10 cm x 10 cm) showed in Figure 1A. A CD1 mouse, mouse surrogate
548 model or tiny audio recorder that broadcasted battle sound was placed in this small box, respectively,
549 about six minutes to test the avoidance behaviors of observational mice and control mice as an index
550 of the fear memories specific to CD1 mouse or battle sound. During this test, the battle sounds about
551 one minute were given three times with one-minute intervals, which was controlled by the Bluetooth.
552 The area within five centimeters around this small box was defined to be an interaction zone (Figure
553 1A, B and D). The stay duration of C57 mice within the interaction zone was named as the interaction
554 time. The EPM consisted of two open arms (30 cm x 5 cm) crossly opposite to two closed arms (30cm
555 × 5cm × 15.25 cm). These arms extended from a central platform (5 cm × 5 cm). The EPM was located
556 40 cm above the floor. The mice were placed in this central platform of the EPM in face to open arms
557 for the test of their anxious state. The measurements of C57 mouse behavioral tests about the time in

558 open arms and the interaction time were analyzed by a Matlab. The detail methods were described in
559 our previous studies (*7, 21, 60, 61, 69*). The timeline for our experiments is presented in Figure 1A.
560 **Anterograde neural tracing**: To trace the formations and changes of neural circuits in control and
561 observational mice with fear memory induced by psychological traumas, we applied adeno-associated
562 viruses (AAV) as a vector that carried genes of encoding fluorescent proteins for an anterograde neural
563 tracing. AAV2/8-CMV-tdTomato-WPRE, AAV2/8-CMV-EBFP2-WPRE and AAV2/8-CMV-EGFP-3xFLAG-
564 WPRE were ordered from OBiO Technology (Shanghai, China) to track RFP-labelled, BFP-labelled and
565 GFP-labelled axons, respectively. The titers of these viral vectors were in a range of 5-6x10^{12} genome
566 copies/ml. All of viral vectors had been aliquoted into 200 µl EP tubes and stored at -80℃ until they
567 were used. The locations for the microinjection of these AAVs as the original areas of neuronal axons
568 and for the confocal scanning of cellular images as the target areas were based on a mouse brain map
569 (*145*).
570 In tracing axon and synapse interconnections between the visual cortex and the auditory cortex
571 in observational and control mice, 0.3 µL AAV-CMV-tdTomato was microinjected into the visual cortex
572 (2.50 mm posterior to the bregma, 2.50 mm lateral to the middle line and 0.35 mm depth away from
573 the cortical surface), and 0.3 µL AAV -CMV-BFP was microinjected into the auditory cortex (2.10 mm
574 posterior to the bregma, 3.80 mm lateral to the middle line and 0.65 mm depth away from the cortical
575 surface) in observers three days before they witnessed the resident/intruder paradigm and in controls
576 before they were placed neighboring the resident-included cage as well as three weeks before neural
577 tracing was done under the confocal microscopy. The microinjections of AAVs in cerebral cortices were
578 conducted by using glass pipettes. The microinjection quantities and durations were controlled by the
579 microsyringe system held with three-dimensional stereotaxic apparatus (RWD Life Science, Shenzhen,

China). Glass pipettes with low interior pressure were reserved at the injection sites no less than 25 minutes before withdrawing from mouse brains. In the principle, the injected AAV-CMV-tdTomato or AAV-CMV- BFP in cerebral cortices was uptaken by the somata of these cortical neurons to express red or blue fluorescent proteins, and subsequently transported toward their axonal terminals and boutons, so that the somata of neurons as the original areas and their projected axons as the target areas were tracked in an anterograde manner. The axon boutons and the contacts between the axon boutons and the dendritic spines of visual or auditory cortical neurons in target areas indicate the axons projected and the synapses formed. The new synapses plus the innate synapses convergently onto auditory and visual cortical neurons indicate that these neurons are recruited as the associative memory neurons to encode battle images and sounds. It is noteworthy that the transfection efficiency of AAVs in cerebral cortices is sufficient for neural tracing. The averaged percentage of AAV transfected neurons is similar to the averaged percentage of cFos-labelled neurons, implying AAV transfections to the active neurons (*64*).

The microinjection of AAV-CMV-tdTomato and AAV-CMV-BFP in the visual cortex and the auditory cortex, respectively, was also used to track the convergent synapse innervations by their axon boutons on the dendritic spines of prefrontal cortical neurons. AAV-vectors transfected neurons in the injection areas expressed their carried-genes and fluorescent proteins. Subsequently, the fluorescent proteins produced in neuronal somata were transported over entire axons in an anterograde manner, such that their axon boutons and terminals labelled by these fluorescent proteins were detected in target areas. The contacts between the axon boutons and the dendritic spines of medial prefrontal cortical neurons were deemed as the synapse contacts. The raised contacts in experiments included the newly formed synapse contacts. Those medial prefrontal cortical neurons with the convergent synapses newly from

602 the visual cortex and the auditory cortex were presumably associative memory neurons (*21, 64, 86-88,*
603 *90*).
604 To track the axon boutons and their innervated synapses in intramodal cortices, 0.3 μL AAV- CMV
605 -tdTomato, 0.3 μL AAV-CMV-BFP and 0.3 μL AAV-CMV-GFP were microinjected in the visual cortex (the
606 location above), the auditory cortex (the location above) and the medial prefrontal cortex (1.70 mm
607 anterior to the bregma, 0.30 mm lateral to the middle line and 1.30 mm depth away from the dorsal
608 cortical surface), respectively. In the scanning by a confocal microscopy, the RFP-labelled axon boutons
609 and their innervated contacts in the visual cortex, the BFP-labelled axon boutons and their innervated
610 contacts in the auditory cortex, and the GFP-labelled axon boutons and their innervated contacts in
611 the medial prefrontal cortex were thought to be intramodal in nature (*109*).
612 The face to a resident/intruder paradigm or the control was conducted three days after surgical
613 operations and microinjections in order to allow C57 mice recovery from operations. In the next two
614 weeks, the fluorescent proteins expressed in neuronal somata were transported to entire axons, axon
615 boutons/terminals along with stress-induced axon elongations. At last, the mice were anesthetized by
616 the intraperitoneal injections of pentobarbital sodium (60 mg/kg) and perfused through left ventricle
617 with 25 ml 0.01M phosphate buffer solution (PBS) followed by 25 ml 4% paraformaldehyde until their
618 bodies were rigid. The brains were quickly isolated and soaked in 4% paraformaldehyde for a fixation
619 about 24 hours. The cerebral brains were sliced by the vibratome in a series of coronal sections with a
620 thickness of 100 μm in the PBS. These slices were air-dried and cover-slipped with 50% glycerin in the
621 PBS. The images about neurons, dendrites, spines and axonal boutons were taken and collected at a
622 60X lens for high magnification under the confocal microscope (Nikon A1R plus, Japan). The anatomic

623 images of the cerebral brain were taken by a 4X lens for a low magnification under this confocal
624 microscope.

625 In C57BL/6JThy1-YFP mice, postsynaptic neuron dendrites and spines were labelled by the YFP.
626 The presynaptic axon boutons whose somata were infected AAV were labelled by BFP, RFP or GFP. The
627 wavelength of the excitation laser-beam 561 nm was utilized to activate the RFP. The wavelength of
628 the excitation laser-beam 488 was applied to activate the GFP. The wavelength of the excitation laser-
629 beam 405 nm was used to activate the BFP. The wavelengths of the emission spectra of the BFP, GFP,
630 YFP and RFP are 412-482 nm, 492-512 nm, 522-552 nm and 572-652 nm, respectively. Those contacts
631 between yellow dendritic spines and red, blue or green axonal boutons with less than 0.1 μm space
632 cleft were presumed to be the chemical synapses. The images of dendritic spines, axon boutons and
633 synapse contacts were analyzed quantitatively by ImageJ and Imaris (*86-88, 90*). Associative memory
634 neurons were accepted by detecting two sources of boutons on the dendritic spines of YFP-labelled
635 cortical neurons.

636 **Electrophysiology *in vivo***: Before the electrophysiological recording of visual, auditory or medial
637 prefrontal cortical neurons *in vivo*, the mice in control group or observer group were anesthetized by
638 intraperitoneal injections of pentobarbital sodium (60 mg/kg) for surgical operations after the control
639 period or the training paradigms had been conducted. The body temperature was kept at 37 °C by a
640 computer-controlled heating blanket. The craniotomy (1 mm in diameter) was done on the mouse
641 skull above the left sides of the visual cortex (2.50 mm posterior to the bregma and 2.50 mm lateral to
642 the midline), the auditory cortex (2.10 mm posterior to the bregma and 3.8 mm lateral to the midline)
643 or the medial prefrontal cortex (1.7 mm anterior to the bregma and 0.3 mm lateral to a midline). The
644 locations for recordings were based on mouse brain map (*145*). Electrophysiological recordings to the

645 cortical neurons *in vivo* were conducted in the mice under light anesthetic condition with a withdrawal
646 reflex by pinching, the eyelid blinking reflex by air-puffing and the muscle relax. The electrical
647 discharges of unitary cortical neurons were recorded in layers IV-V of these cortices by using the glass
648 pipettes filled with the standard solution (150 mM NaCl, 3.5 mM KCl and 5 mM HEPES). The resistance
649 of the recording pipettes was 40-50MΩ. The electrical signals from these cortical neurons in their
650 spontaneous spikes and their evoked spikes in response to battle sounds or battle images were
651 recorded and acquired by an AxoClamp-2B amplifier and a Digidata 1322A, and were analyzed by the
652 pClamp 10 system (Axon Instrument Inc. CA, USA). These spiking signals were digitized at 20 kHz and
653 filtered by a low-pass at 5 kHz. A 100-3000 Hz band-pass filter and a second-order Savitzky-Golay filter
654 were used to isolate spike signals. Spike frequencies were quantitatively analyzed (*86-88, 90*). Battle
655 images and battle sounds in a resident/ intruder paradigm, housing environment sounds and
656 floral-pattern images were given for 30 seconds. The visual stimulus apparatus was an 8 cm x 16 cm
657 LCD monitor (BOE Beijing, China) with 2400 x 1080 pixels in the resolution, the refresh rate of 60 Hz
658 and the mean luminance of 30 cd/m^2. The screen was positioned 12 cm from the left eye occupying
659 ~36˚ x 68˚ degrees of visual space. The auditory stimulus was delivered by a speaker (Huawei,
660 Shenzhen, China) in a range of sound intensity from 60-80 dB and a range of frequencies at 220 Hz-22
661 kHz. The speaker was positioned 25 cm from the left ear.
662 Normalized spike frequency in response to one of stimuli was the number of the spike frequency
663 in response to the stimulus in 30 seconds divided by spontaneous discharge frequency in 30 seconds
664 before the stimulus. When the ratio reached 1.5 or above, these cortical neurons were deemed as the
665 response to this stimulus. Associative memory neurons (AMN) were accepted by detecting a situation

666 that those cortical neurons responded to both stimulations. The identification of associative memory
667 neurons versus those active neurons in response to a stimulus is presented in Figure S6.
668 **KiF1a knockdown by shRNA carried by AAV:** In the study of the role of axon transportation in
669 the elongation of axons and the formation of new synapse innervations, KiF1a, one of the motor
670 proteins for axon transportation (*95-97, 99-101*) was knocked down in the medial prefrontal cortex by
671 microinjecting short-hairpin RNA (shRNA) specific to KiF1a mRNA that was carried by AAV vectors
672 (AAV-U6-sh*KiF1a*-GFP) into these cortical areas in one subgroup of observational mice. The piece of
673 scramble sequence carried by AAV (AAV-U6-scramble-EGFP) as the control was injected in the medial
674 prefrontal cortex in another subgroup of observational mice. These virus vectors were designed by
675 BrainVTA (Wuhan, China). The microinjections were operated five days before training protocols for
676 effective AAV transfection and gene knockdown (Figure S3). This approach suppresses the expression
677 of KiF1a mRNA and protein in the medial prefrontal cortical neurons, the formation of new synapse
678 innervations from visual and auditory cortices and the recruitment of associative memory neurons in
679 the medial prefrontal cortex.
680 With the approach of KiF1a knockdown in the medial prefrontal cortex (Figure S3), the
681 behavioral tests, AAV-mediated neural tracing and electrophysiological recording *in vivo* were done to
682 assess the effects of the KiF1a knockdown on fear memory, synapse formation and associative
683 memory neuron recruitment in the medial prefrontal cortex. Specifically, the encoding ability of its
684 neurons in response to battle sounds and the battle images were analyzed and compared in two
685 subgroups. The effects of shRNA specific to the KiF1a knockdown on new synapse formation and
686 associative memory neuron recruitment were ensured if the numbers of new synapse contacts and

687 associative memory neurons in KiF1a-knockdown mice were lowered significantly in comparison with
688 scramble control mice.

689 **RNA extraction and quantitative real-time PCR analysis of KiF1a**: The mPFC regions in the brain
690 were isolated and harvested from control mice and observational mice twelve days after treatments.
691 mPFC tissues in observational mice in the subgroups of KiF1a-KD and scramble control were harvested
692 about three weeks after the bilateral injections with AAV2/9-U6-shRNA(KiF1a)-CMV-EGFP-SV40 pA or
693 AAV2/9-U6-shRNA(scramble)-CMV-EGFP-SV40 pA (0.3 μl per side). Total RNA was isolated by using the
694 FastPure Cell/Tissue Total RNA Isolation Kit V2 (Vazyme, Nanjing, China). The HiScript IV RT SuperMix
695 for qPCR kit (Vazyme, Nanjing, China) was used to reversely transcribe RNAs to complementary DNAs
696 (cDNA). qRT-PCR was performed on Applied Biosystems® QuantStudio™ 7 Flex (ABI, USA) with ChamQ
697 Universal SYBR qPCR Master mix (Vazyme, Nanjing, China). The primer and amplicon specificity were
698 ensured to be effective by analyzing melt curves and blasting products, DNA sequence. With *GADPH*
699 as the internal reference, the method of 2-ΔΔCT was used to determine the relative values of mRNA
700 expression of *KiF1a* gene. The sequences of PCR primers were 5'- CACCACTATTGTCAACCCCAAA-3' and
701 5'- CCCCAATGTCCCTGTAGACCT-3' for *KiF1a* as well as 5'-AGGTCGGTGTGAACGGATTTG-3' and
702 5'-TGTAGACCATGTAGTTGAGGTCA-3' for GADPH.

703 **Immunofluorescence:** The mice were anesthetized by the intraperitoneal injections of urethane
704 (1.5g/kg) and perfused via the left ventricle with ice-cold 25 ml 0.1M phosphate buffer solution (PBS,
705 pH=7.4) followed by 25 ml 4% paraformaldehyde until their bodies were rigid. The brains of such mice
706 were postfixed with 4% paraformaldehyde for 12 hours and then kept in the PBS. The cerebral brains
707 were sliced by a vibratome in a series of coronal slices with 30 μm thickness of in the PBS. The slices
708 were washed in the PBS, blocked by a buffer solution containing 5% goat serum and 0.3% Triton X-100

709 for 2 hours at the room temperature (22-25°C), incubated with the buffer solution that contained the
710 primary antibody (Anti-KiF1a, Proteintech, 24841-1-AP in China) in 1% bull serum albumin (free for
711 KiF1a staining) and 0.3% Triton X-100 at 4°C for overnight. After rinsed three times in the PBS, these
712 slices were incubated with the secondary antibody for two hours and then, if necessary, incubated
713 with 4',6-diamidino-2- phenylindole for 5 minutes at room temperature. The secondary antibody for
714 the staining was goat anti-rabbit antibody conjugated with Alexa Fluor 647 (CST, 4414). These slices
715 were lastly rinsed three times, mounted on microscope slides, air-dried and cover-slipped with 50%
716 glycerin in the PBS. The number of fluorescent protein-labelled neurons was counted by Image Fiji.
717 The neurons in different channels were selected by a "threshold" tool. The selected ROI regions were
718 added to ROI manager. An "analyze particles" (size from 1-infinity) tool was used to count the number
719 of those neurons labelled by the KiF1a motor protein and the GFP (lower threshold level at 50, upper
720 threshold level at 255). Images were captured under a confocal laser-scanning microscope (Nikon A1R
721 plus, Japan). The colocalization analysis and merged images were done based on our previous studies
722 (*86-88, 90*).
723 **Statistics**: All data are presented to be arithmetic mean±SEM. The statistical analyses of our data
724 were conducted by using GraphPad Prism 9 (a public software). The one-way ANOVA was used for the
725 statistical comparison of the changes in behaviors, morphology and neuronal activities between those
726 control and observer groups as well as between KiF1a-knockdown and scramble control subgroups in
727 observers. A paired *t*-test was used to compare the activities of associative memory neurons before
728 and after drug application, as well as the encoding ability of associative memory neurons in response
729 to two signals. Chi-square test was used for the statistic comparison of the changes in the number and
730 the percentage of associative memory neurons as well as active neurons in electrophysiological study

among these groups. The P values equally and above 0.05 in the comparisons among the groups were set to be no statistical difference, or vice versa. One asterisk, two asterisks, three asterisks and four asterisks were presented to be P values less than 0.05, 0.01, 0.001 and 0.0001, respectively.

Declarations

Ethics approval and consent to participate: Experiments were done in accordance with guidelines and regulations by the Administration Office of Laboratory Animal in Beijing China. All experiment protocols were approved by Institutional Animal Care and Use Committee in this office at Beijing China (B10831).

Consent for publication: In the publication of this manuscript, no individual' data, such as personal details, images, videos and voice are included. All necessary consent for publication has been secured.

Availability of data, code, and material: The datasets used and analyzed in the current study are available from the corresponding author based on the request without commercial purpose.

Competing interests: All authors declare no competing interest. All authors have read and approved the final version of the manuscript.

Acknowledgements: This study is funded by the Natural Science Foundation of China (81971027 and U2241209) to Jin-Hui Wang.

Authors Contributions: Jiayi Li, Yu Guo, Bingchen Chen, Yun Zhang and Lei Wang contributed to the experiments and data analyses. Jin-Hui Wang contributed to the concept, project design, funding acquisition and paper writing.

753 **References**

754 1. S. Battaglia, Neurobiological advances of learned fear in humans. *Adv Clin Exp Med* **31**,
755 217-221 (2022).
756 2. A. Olsson, K. I. Nearing, E. A. Phelps, Learning fears by observing others: the neural systems of
757 social fear transmission. *Soc Cogn Affect Neurosci* **2**, 3-11 (2007).
758 3. A. Olsson, E. A. Phelps, Social learning of fear. *Nat Neurosci* **10**, 1095-1102 (2007).
759 4. E. Baldi, C. Bucherelli, Brain sites involved in fear memory reconsolidation and extinction of
760 rodents. *Neurosci Biobehav Rev* **53**, 160-190 (2015).
761 5. L. Coutellier, T. B. Usdin, Enhanced long-term fear memory and increased anxiety and
762 depression-like behavior after exposure to an aversive event in mice lacking TIP39 signaling.
763 *Behav Brain Res* **222**, 265-269 (2011).
764 6. A. Desmedt, A. Marighetto, P. V. Piazza, Abnormal Fear Memory as a Model for Posttraumatic
765 Stress Disorder. *Biol Psychiatry* **78**, 290-297 (2015).
766 7. K. Du, W. Lu, Y. Sun, J. Feng, J. H. Wang, mRNA and miRNA profiles in the nucleus accumbens
767 are related to fear memory and anxiety induced by physical or psychological stress. *J Psychiatr*
768 *Res* **118**, 44-65 (2019).
769 8. I. Izquierdo, C. R. Furini, J. C. Myskiw, Fear Memory. *Physiol Rev* **96**, 695-750 (2016).
770 9. S. R. Makkar, S. Q. Zhang, J. Cranney, Behavioral and neural analysis of GABA in the
771 acquisition, consolidation, reconsolidation, and extinction of fear memory.
772 *Neuropsychopharmacology* **35**, 1625-1652 (2010).
773 10. C. A. Orsini, S. Maren, Neural and cellular mechanisms of fear and extinction memory
774 formation. *Neurosci Biobehav Rev* **36**, 1773-1802 (2012).
775 11. R. G. Parsons, K. J. Ressler, Implications of memory modulation for post-traumatic stress and
776 fear disorders. *Nat Neurosci* **16**, 146-153 (2013).
777 12. D. M. Warthen, B. J. Wiltgen, I. Provencio, Light enhances learned fear. *Proc Natl Acad Sci U S*
778 *A* **108**, 13788-13793 (2011).
779 13. G. Thrall, D. Lane, D. Carroll, G. Y. Lip, A systematic review of the effects of acute psychological
780 stress and physical activity on haemorheology, coagulation, fibrinolysis and platelet reactivity:
781 Implications for the pathogenesis of acute coronary syndromes. *Thromb Res* **120**, 819-847

782 (2007).
783 14. J. H. Wang, Searching basic units in memory traces: associative memory cells. *F1000Res* **8**,
784 457 (2019).
785 15. R. Zeitlin *et al.*, Cotinine enhances the extinction of contextual fear memory and reduces
786 anxiety after fear conditioning. *Behav Brain Res* **228**, 284-293 (2012).
787 16. D. de Quervain, L. Schwabe, B. Roozendaal, Stress, glucocorticoids and memory: implications
788 for treating fear-related disorders. *Nat Rev Neurosci* **18**, 7-19 (2017).
789 17. A. Flores, M. A. Fullana, C. Soriano-Mas, R. Andero, Lost in translation: how to upgrade fear
790 memory research. *Mol Psychiatry* **23**, 2122-2132 (2018).
791 18. S. Maren, Seeking a spotless mind: extinction, deconsolidation, and erasure of fear memory.
792 *Neuron* **70**, 830-845 (2011).
793 19. R. M. Shansky, E. M. Greiner, A covert cortical ensemble for learned fear suppression.
794 *Neuropsychopharmacology* **49**, 1949-1950 (2024).
795 20. J. Sandkuhler, J. Lee, How to erase memory traces of pain and fear. *Trends Neurosci* **36**,
796 343-352 (2013).
797 21. B. Chen *et al.*, Associative memory cells of encoding fear signals and anxiety are recruited by
798 neuroligin-3-mediated synapse formation. *Commun Biol* **7**, 1464 (2024).
799 22. R. Marek, C. Strobel, T. W. Bredy, P. Sah, The amygdala and medial prefrontal cortex: partners
800 in the fear circuit. *J Physiol* **591**, 2381-2391 (2013).
801 23. S. Maren, Pavlovian fear conditioning as a behavioral assay for hippocampus and amygdala
802 function: cautions and caveats. *Eur J Neurosci* **28**, 1661-1666 (2008).
803 24. G. E. Schafe, K. Nader, H. T. Blair, J. E. LeDoux, Memory consolidation of Pavlovian fear
804 conditioning: a cellular and molecular perspective. *Trends Neurosci* **24**, 540-546 (2001).
805 25. G. P. Shumyatsky *et al.*, Identification of a signaling network in lateral nucleus of amygdala
806 important for inhibiting memory specifically related to learned fear. *Cell* **111**, 905-918 (2002).
807 26. T. Agren *et al.*, Disruption of reconsolidation erases a fear memory trace in the human
808 amygdala. *Science* **337**, 1550-1552 (2012).
809 27. S. K. Barot, A. Chung, J. J. Kim, I. L. Bernstein, Functional imaging of stimulus convergence in
810 amygdalar neurons during Pavlovian fear conditioning. *PLoS ONE* **4**, e6156 (2009).

811 28. H. T. Blair, G. E. Schafe, E. P. Bauer, S. M. Rodrigues, J. E. LeDoux, Synaptic plasticity in the
812 lateral amygdala: a cellular hypothesis of fear conditioning. *Learn Mem* **8**, 229-242 (2001).
813 29. R. J. Davidson, Anxiety and affective style: one of prefrontal cortex and amygdala. *Biological*
814 *Psychiatry* **51**, 68-80 (2002).
815 30. C. W. Butler, Y. M. Wilson, J. M. Gunnersen, M. Murphy, Tracking the fear memory engram:
816 discrete populations of neurons within amygdala, hypothalamus, and lateral septum are
817 specifically activated by auditory fear conditioning. *Learn Mem* **22**, 370-384 (2015).
818 31. D. C. Choi *et al.*, Prelimbic cortical BDNF is required for memory of learned fear but not
819 extinction or innate fear. *Proc Natl Acad Sci U S A* **107**, 2675-2680 (2010).
820 32. I. Ehrlich *et al.*, Amygdala inhibitory circuits and the control of fear memory. *Neuron* **62**,
821 757-771 (2009).
822 33. M. Davis, The role of the amygdala in fear and anxiety. *Annual Review of Neuroscience* **15**,
823 353-375 (1992).
824 34. A. E. Dityatev, V. Y. Bolshakov, Amygdala, long-term potentiation, and fear conditioning.
825 *Neuroscientist* **11**, 75-88 (2005).
826 35. S. Duvarci, D. Pare, Amygdala microcircuits controlling learned fear. *Neuron* **82**, 966-980
827 (2014).
828 36. J. P. Fadok, M. Darvas, T. M. K. Dickerson, R. D. Palmiter, Long-Term Memory for Pavlovian
829 Fear Conditioning Requires Dopamine in the Nucleus Accumbens and Basolateral Amygdala.
830 *Plos One* **5**, (2010).
831 37. G. E. Fenton, D. M. Halliday, R. Mason, T. W. Bredy, C. W. Stevenson, Sex differences in learned
832 fear expression and extinction involve altered gamma oscillations in medial prefrontal cortex.
833 *Neurobiol Learn Mem* **135**, 66-72 (2016).
834 38. M. S. Fanselow, G. D. Gale, The amygdala, fear, and memory. *Ann N Y Acad Sci* **985**, 125-134
835 (2003).
836 39. E. J. Kim *et al.*, Dorsal periaqueductal gray-amygdala pathway conveys both innate and
837 learned fear responses in rats. *Proc Natl Acad Sci U S A* **110**, 14795-14800 (2013).
838 40. N. C. Ferrara, S. Trask, S. E. Pullins, F. J. Helmstetter, Regulation of learned fear expression
839 through the MgN-amygdala pathway. *Neurobiol Learn Mem* **185**, 107526 (2021).

840 41. G. Giannotti, J. A. Heinsbroek, A. J. Yue, K. Deisseroth, J. Peters, Prefrontal cortex neuronal
841 ensembles encoding fear drive fear expression during long-term memory retrieval. *Sci Rep* **9**,
842 10709 (2019).
843 42. O. B. Kwon *et al.*, Dopamine Regulation of Amygdala Inhibitory Circuits for Expression of
844 Learned Fear. *Neuron* **88**, 378-389 (2015).
845 43. C. Herry, R. Garcia, Prefrontal cortex long-term potentiation, but not long-term depression, is
846 associated with the maintenance of extinction of learned fear in mice. *J Neurosci* **22**, 577-583
847 (2002).
848 44. M. Heshmati *et al.*, Mefloquine in the nucleus accumbens promotes social avoidance and
849 anxiety-like behavior in mice. *Neuropharmacology* **101**, 351-357 (2016).
850 45. T. Isosaka *et al.*, Htr2a-Expressing Cells in the Central Amygdala Control the Hierarchy
851 between Innate and Learned Fear. *Cell* **163**, 1153-1164 (2015).
852 46. R. Lamprecht, C. R. Farb, S. M. Rodrigues, J. E. LeDoux, Fear conditioning drives profilin into
853 amygdala dendritic spines. *Nat Neurosci* **9**, 481-483 (2006).
854 47. L. Levita, J. W. Dalley, T. W. Robbins, Nucleus accumbens dopamine and learned fear revisited:
855 a review and some new findings. *Behav Brain Res* **137**, 115-127 (2002).
856 48. L. Levita, R. Hoskin, S. Champi, Avoidance of harm and anxiety: A role for the nucleus
857 accumbens. *Neuroimage* **62**, 189-198 (2012).
858 49. S. Li, J. H. Kim, R. Richardson, Differential involvement of the medial prefrontal cortex in the
859 expression of learned fear across development. *Behav Neurosci* **126**, 217-225 (2012).
860 50. M. Maroun, Medial prefrontal cortex: multiple roles in fear and extinction. *Neuroscientist* **19**,
861 370-383 (2013).
862 51. J. D. Runyan, A. N. Moore, P. K. Dash, A role for prefrontal cortex in memory storage for trace
863 fear conditioning. *J Neurosci* **24**, 1288-1295 (2004).
864 52. D. Pare, Mechanisms of Pavlovian fear conditioning: has the engram been located? *Trends*
865 *Neurosci* **25**, 436-437; discussion 437-438 (2002).
866 53. J. A. Silvers *et al.*, An exploration of amygdala-prefrontal mechanisms in the intergenerational
867 transmission of learned fear. *Dev Sci* **24**, e13056 (2021).
868 54. R. C. Twining, J. E. Vantrease, S. Love, M. Padival, J. A. Rosenkranz, An intra-amygdala circuit

869 specifically regulates social fear learning. *Nat Neurosci* **20**, 459-469 (2017).
870 55. O. Berton *et al.*, Essential role of BDNF in the mesolimbic dopamine pathway in social defeat
871 stress. *Science* **311**, 864-868 (2006).
872 56. K. Bjorkqvist, Social defeat as a stressor in humans. *Physiol Behav* **73**, 435-442 (2001).
873 57. C. Hammels *et al.*, Defeat stress in rodents: From behavior to molecules. *Neurosci Biobehav*
874 *Rev* **59**, 111-140 (2015).
875 58. M. Martinez, A. Calvo-Torrent, M. A. Pico-Alfonso, Social Defeat and Subordination as Models
876 of Social Stress in Laboratory Rodents: A Review. *Aggressive Behavior* **24**, 241-256 (1998).
877 59. Y. Lu, J. Yang, J. Sun, W. Lu, J. H. Wang, mRNA and miRNA profiles in the nucleus accumbens
878 are associated with psychological stress-induced susceptible and resilient mice. *Pharmacol*
879 *Biochem Behav* **199**, 173062 (2020).
880 60. J. Sun *et al.*, mRNA and microRNA Profiles in the Amygdala Are Relevant to Susceptibility and
881 Resilience to Psychological Stress Induced in Mice. *J Mol Neurosci* **70**, 1771-1796 (2020).
882 61. Y. Sun, W. Lu, K. Du, J. H. Wang, microRNA and mRNA profiles in the amygdala are relevant to
883 fear memory induced by physical or psychological stress. *J Neurophysiol* **122**, 1002-1022
884 (2019).
885 62. N. M. Tsankova *et al.*, Sustained hippocampal chromatin regulation in a mouse model of
886 depression and antidepressant action. *Nat Neurosci* **9**, 519-525 (2006).
887 63. J. H. Wang, *Associative memory cells: basic units of memory trace*. J. H. Wang, Ed., Associative
888 memory cells: basic units of memory trace (Springer Nature, Springer, ed. the first, 2019).
889 64. Y. Zhang *et al.*, Auditory cortical neurons are recruited to encode fear signals and anxiety by
890 neuroligin-3-mediated synapse formation. *Transl Psychiatry* **15**, 140 (2025).
891 65. L. A. Gouty-Colomer *et al.*, Arc expression identifies the lateral amygdala fear memory trace.
892 *Mol Psychiatry* **21**, 364-375 (2016).
893 66. R. Lamprecht, S. Dracheva, S. Assoun, J. E. LeDoux, Fear conditioning induces distinct patterns
894 of gene expression in lateral amygdala. *Genes Brain Behav* **8**, 735-743 (2009).
895 67. H. C. Pape, O. Stork, Genes and mechanisms in the amygdala involved in the formation of fear
896 memory. *Ann N Y Acad Sci* **985**, 92-105 (2003).
897 68. I. B. Zovkic, J. D. Sweatt, Epigenetic mechanisms in learned fear: implications for PTSD.

898 *Neuropsychopharmacology* **38**, 77-93 (2013).
899 69. J. Yang *et al.*, Correction to: mRNA and microRNA profiles are associated with stress
900 susceptibility and resilience induced by psychological stress in the prefrontal cortex.
901 *Psychopharmacology (Berl)* **237**, 3095 (2020).
902 70. A. Meulders, Fear in the context of pain: Lessons learned from 100 years of fear conditioning
903 research. *Behav Res Ther* **131**, 103635 (2020).
904 71. J. Debiec, A. Olsson, Social Fear Learning: from Animal Models to Human Function. *Trends*
905 *Cogn Sci* **21**, 546-555 (2017).
906 72. A. Olsson, E. A. Phelps, Learned fear of "unseen" faces after Pavlovian, observational, and
907 instructed fear. *Psychol Sci* **15**, 822-828 (2004).
908 73. A. Olsson, E. Knapska, B. Lindstrom, The neural and computational systems of social learning.
909 *Nat Rev Neurosci* **21**, 197-212 (2020).
910 74. A. Burgos-Robles, K. M. Gothard, M. H. Monfils, A. Morozov, A. Vicentic, Conserved features
911 of anterior cingulate networks support observational learning across species. *Neurosci*
912 *Biobehav Rev* **107**, 215-228 (2019).
913 75. Y. Pan, M. C. Vinding, L. Zhang, D. Lundqvist, A. Olsson, A Brain-To-Brain Mechanism for Social
914 Transmission of Threat Learning. *Adv Sci (Weinh)* **10**, e2304037 (2023).
915 76. A. Louzolo *et al.*, Enhanced Instructed Fear Learning in Delusion-Proneness. *Front Psychol* **13**,
916 786778 (2022).
917 77. I. Undeger, R. M. Visser, A. Olsson, Neural Pattern Similarity Unveils the Integration of Social
918 Information and Aversive Learning. *Cereb Cortex* **30**, 5410-5419 (2020).
919 78. L. Dixsaut, J. Graff, The Medial Prefrontal Cortex and Fear Memory: Dynamics, Connectivity,
920 and Engrams. *Int J Mol Sci* **22**, (2021).
921 79. I. Hasegawa, Neural mechanisms of memory retrieval: role of the prefrontal cortex. *Rev*
922 *Neurosci* **11**, 113-125 (2000).
923 80. Y. Huang, A. Matysiak, P. Heil, R. Konig, M. Brosch, Persistent neural activity in auditory cortex
924 is related to auditory working memory in humans and nonhuman primates. *Elife* **5**, (2016).
925 81. S. J. D. Lawrence *et al.*, Laminar Organization of Working Memory Signals in Human Visual
926 Cortex. *Curr Biol* **28**, 3435-3440 e3434 (2018).

927 82. E. Likhtik, J. M. Stujenske, M. A. Topiwala, A. Z. Harris, J. A. Gordon, Prefrontal entrainment of
928 amygdala activity signals safety in learned fear and innate anxiety. *Nat Neurosci* **17**, 106-113
929 (2014).
930 83. J. H. Yoon, C. E. Curtis, M. D'Esposito, Differential effects of distraction during working
931 memory on delay-period activity in the prefrontal cortex and the visual association cortex.
932 *Neuroimage* **29**, 1117-1126 (2006).
933 84. L. Yu *et al.*, The causal role of auditory cortex in auditory working memory. *Elife* **10**, (2021).
934 85. M. Vasconcelos, D. J. Stein, R. M. de Almeida, Social defeat protocol and relevant biomarkers,
935 implications for stress response physiology, drug abuse, mood disorders and individual stress
936 vulnerability: a systematic review of the last decade. *Trends Psychiatry Psychother* **37**, 51-66
937 (2015).
938 86. J. Feng *et al.*, Barrel cortical neuron integrates triple associated signals for their memory
939 through receiving epigenetic-mediated new synapse innervations. *Cerebral Cortex* **27**,
940 5858-5871 (2017).
941 87. Z. Gao *et al.*, Coactivations of barrel and piriform cortices induce their mutual synapse
942 innervations and recruit associative memory cells. *Brain Res*, 146333 (2019).
943 88. Z. Lei *et al.*, Synapse innervation and associative memory cell are recruited for integrative
944 storage of whisker and odor signals in the barrel cortex through miRNA-mediated processes. .
945 *Frontiers in Cellular Neuroscience* **11**, 1-11 (2017).
946 89. R. Wu, S. Cui, J. H. Wang, miRNA-324/-133a essential for recruiting new synapse innervations
947 and associative memory cells in coactivated sensory cortices. *Neurobiol Learn Mem* **172**,
948 107246 (2020).
949 90. Y. Xu, T. L. Cui, J. Y. Li, B. Chen, J. H. Wang, Associative memory neurons of encoding
950 multi-modal signals are recruited by neuroligin-3-mediated new synapse formation. *Elife* **12**,
951 (2023).
952 91. D. Wang *et al.*, Neurons in the barrel cortex turn into processing whisker and odor signals: a
953 cellular mechanism for the storage and retrieval of associative signals. *Front Cell Neurosci* **9**,
954 320 (2015).
955 92. P. G. Anastasiades, A. G. Carter, Circuit organization of the rodent medial prefrontal cortex.

956 *Trends Neurosci* **44**, 550-563 (2021).
957 93. J.-H. Wang, J. Feng, W. Lu, H. Xiao, Prefrontal Cortical Neurons Are Recruited As Secondary
958 Associative Memory Cells for Associative Memory and Cognition. *Biophysical Journal* **114**,
959 155a (2018).
960 94. J. H. Wang, J. Feng, H. Xiao, Y. Xu, Secondary associative memory cells and their plasticity in
961 the prefrontal cortex. *Biophysical Journal* **116**, 427a (2019).
962 95. N. Hirokawa, R. Nitta, Y. Okada, The mechanisms of kinesin motor motility: lessons from the
963 monomeric motor KIF1A. *Nat Rev Mol Cell Biol* **10**, 877-884 (2009).
964 96. J. R. Lee *et al.*, Characterization of the movement of the kinesin motor KIF1A in living cultured
965 neurons. *J Biol Chem* **278**, 2624-2629 (2003).
966 97. R. Nitta, M. Kikkawa, Y. Okada, N. Hirokawa, KIF1A alternately uses two loops to bind
967 microtubules. *Science* **305**, 678-683 (2004).
968 98. S. Niwa *et al.*, Autoinhibition of a Neuronal Kinesin UNC-104/KIF1A Regulates the Size and
969 Density of Synapses. *Cell Rep* **16**, 2129-2141 (2016).
970 99. Y. Okada, H. Yamazaki, Y. Sekine-Aizawa, N. Hirokawa, The neuron-specific kinesin superfamily
971 protein KIF1A is a unique monomeric motor for anterograde axonal transport of synaptic
972 vesicle precursors. *Cell* **81**, 769-780 (1995).
973 100. Y. Okada, N. Hirokawa, A processive single-headed motor: kinesin superfamily protein KIF1A.
974 *Science* **283**, 1152-1157 (1999).
975 101. Y. Okada, H. Higuchi, N. Hirokawa, Processivity of the single-headed kinesin KIF1A through
976 biased binding to tubulin. *Nature* **424**, 574-577 (2003).
977 102. D. Oriola, S. Roth, M. Dogterom, J. Casademunt, Formation of helical membrane tubes around
978 microtubules by single-headed kinesin KIF1A. *Nat Commun* **6**, 8025 (2015).
979 103. M. Rierola, N. I. Trushina, M. Holtmannspotter, R. Kurre, L. Bakota, Lattice light-sheet
980 microscopy and evaluation of dendritic transport in cultured hippocampal tissue reveal high
981 variability in mobility of the KIF1A motor domain and entry into dendritic spines. *Brain Res*
982 *Bull* **194**, 13-22 (2023).
983 104. H. Shin *et al.*, Association of the kinesin motor KIF1A with the multimodular protein
984 liprin-alpha. *J Biol Chem* **278**, 11393-11401 (2003).

985 105. R. Stucchi *et al.*, Regulation of KIF1A-Driven Dense Core Vesicle Transport: Ca(2+)/CaM
986 Controls DCV Binding and Liprin-alpha/TANC2 Recruits DCVs to Postsynaptic Sites. *Cell Rep* **24**,
987 685-700 (2018).
988 106. Y. V. Zhang *et al.*, The KIF1A homolog Unc-104 is important for spontaneous release,
989 postsynaptic density maturation and perisynaptic scaffold organization. *Sci Rep* **7**, 38172
990 (2017).
991 107. M. Kondo, Y. Takei, N. Hirokawa, Motor protein KIF1A is essential for hippocampal
992 synaptogenesis and learning enhancement in an enriched environment. *Neuron* **73**, 743-757
993 (2012).
994 108. Y. Tanaka *et al.*, The Molecular Motor KIF1A Transports the TrkA Neurotrophin Receptor and
995 Is Essential for Sensory Neuron Survival and Function. *Neuron* **90**, 1215-1229 (2016).
996 109. J. Y. Li, Y. Xu, D. G. Wang, J. H. Wang, The interconnection and function of associative memory
997 neurons are upregulated for memory strengthening. *Front Neural Circuits* **17**, 1189907
998 (2023).
999 110. F. Yan *et al.*, Coordinated plasticity between barrel cortical glutamatergic and GABAergic
1000 neurons during associative memory. *Neural Plasticity* **2016**, 1-20 (2016).
1001 111. A. M. Craig, Y. Kang, Neurexin-neuroligin signaling in synapse development. *Curr Opin*
1002 *Neurobiol* **17**, 43-52 (2007).
1003 112. M. F. Lise, A. El-Husseini, The neuroligin and neurexin families: from structure to function at
1004 the synapse. *Cell Mol Life Sci* **63**, 1833-1849 (2006).
1005 113. T. C. Sudhof, Synaptic Neurexin Complexes: A Molecular Code for the Logic of Neural Circuits.
1006 *Cell* **171**, 745-769 (2017).
1007 114. M. Uchigashima, A. Cheung, K. Futai, Neuroligin-3: A Circuit-Specific Synapse Organizer That
1008 Shapes Normal Function and Autism Spectrum Disorder-Associated Dysfunction. *Front Mol*
1009 *Neurosci* **14**, 749164 (2021).
1010 115. J. Bigelow, B. Rossi, A. Poremba, Neural correlates of short-term memory in primate auditory
1011 cortex. *Front Neurosci* **8**, 250 (2014).
1012 116. M. Colombo, M. R. D'Amato, H. R. Rodman, C. G. Gross, Auditory association cortex lesions
1013 impair auditory short-term memory in monkeys. *Science* **247**, 336-338 (1990).

1014 117. C. Gilbert, M. Ito, M. Kapadia, G. Westheimer, Interactions between attention, context and
1015 learning in primary visual cortex. *Vision Res* **40**, 1217-1226 (2000).
1016 118. Y. Gottlieb, E. Vaadia, M. Abeles, Single unit activity in the auditory cortex of a monkey
1017 performing a short term memory task. *Exp Brain Res* **74**, 139-148 (1989).
1018 119. H. Nomura *et al.*, Memory formation and retrieval of neuronal silencing in the auditory cortex.
1019 *Proc Natl Acad Sci U S A* **112**, 9740-9744 (2015).
1020 120. P. Phylactou, A. Traikapi, M. Papadatou-Pastou, N. Konstantinou, Sensory recruitment in
1021 visual short-term memory: A systematic review and meta-analysis of sensory visual cortex
1022 interference using transcranial magnetic stimulation. *Psychon Bull Rev* **29**, 1594-1624 (2022).
1023 121. H. Super, Cognitive processing in the primary visual cortex: from perception to memory. *Rev*
1024 *Neurosci* **13**, 287-298 (2002).
1025 122. V. van de Ven, A. T. Sack, Transcranial magnetic stimulation of visual cortex in memory:
1026 cortical state, interference and reactivation of visual content in memory. *Behav Brain Res* **236**,
1027 67-77 (2013).
1028 123. M. Tsanov, D. Manahan-Vaughan, Synaptic plasticity from visual cortex to hippocampus:
1029 systems integration in spatial information processing. *Neuroscientist* **14**, 584-597 (2008).
1030 124. N. M. Weinberger, Specific long-term memory traces in primary auditory cortex. *Nature*
1031 *Reviews of Neuroscience* **5**, 279-290 (2004).
1032 125. C. L. Beeman, P. S. Bauer, J. L. Pierson, J. J. Quinn, Hippocampus and medial prefrontal cortex
1033 contributions to trace and contextual fear memory expression over time. *Learn Mem* **20**,
1034 336-343 (2013).
1035 126. O. Y. Chao, M. A. de Souza Silva, Y. M. Yang, J. P. Huston, The medial prefrontal cortex -
1036 hippocampus circuit that integrates information of object, place and time to construct
1037 episodic memory in rodents: Behavioral, anatomical and neurochemical properties. *Neurosci*
1038 *Biobehav Rev* **113**, 373-407 (2020).
1039 127. J. Courtin, T. C. Bienvenu, E. O. Einarsson, C. Herry, Medial prefrontal cortex neuronal circuits
1040 in fear behavior. *Neuroscience* **240**, 219-242 (2013).
1041 128. D. R. Euston, A. J. Gruber, B. L. McNaughton, The role of medial prefrontal cortex in memory
1042 and decision making. *Neuron* **76**, 1057-1070 (2012).

1043 129. M. R. Milad, G. J. Quirk, Neurons in medial prefrontal cortex signal memory for fear extinction.
1044 *Nature* **420**, 70-74 (2002).
1045 130. J. F. Morici, P. Bekinschtein, N. V. Weisstaub, Medial prefrontal cortex role in recognition
1046 memory in rodents. *Behav Brain Res* **292**, 241-251 (2015).
1047 131. Z. Gao *et al.*, Associations of unilateral whisker and olfactory signals induce synapse
1048 formation and memory cell recruitment in bilateral barrel cortices: cellular mechanism for
1049 unilateral training toward bilateral memory. *Frontiers in Cellular Neuroscience* **10**, 1-16
1050 (2016).
1051 132. Y. Liu *et al.*, Piriform cortical glutamatergic and GABAergic neurons express coordinated
1052 plasticity for whisker-induced odor recall. *Oncotarget* **8**, 95719-95740 (2017).
1053 133. S. A. Josselyn, S. Kohler, P. W. Frankland, Finding the engram. *Nat Rev Neurosci* **16**, 521-534
1054 (2015).
1055 134. S. A. Josselyn, S. Tonegawa, Memory engrams: Recalling the past and imagining the future.
1056 *Science* **367**, (2020).
1057 135. J. I. Kim, H. Y. Cho, J. H. Han, B. K. Kaang, Which Neurons Will Be the Engram - Activated
1058 Neurons and/or More Excitable Neurons? *Exp Neurobiol* **25**, 55-63 (2016).
1059 136. H. Abe, T. S. Nowak, Jr., Induced hippocampal neuron protection in an optimized gerbil
1060 ischemia model: insult thresholds for tolerance induction and altered gene expression
1061 defined by ischemic depolarization. *J Cereb Blood Flow Metab* **24**, 84-97 (2004).
1062 137. P. M. Bokesch, J. E. Marchand, C. S. Connelly, W. H. Wurm, R. M. Kream, Dextromethorphan
1063 inhibits ischemia-induced c-fos expression and delayed neuronal death in hippocampal
1064 neurons. *Anesthesiology* **81**, 470-477 (1994).
1065 138. M. Kiessling, P. Gass, Immediate early gene expression in experimental epilepsy. *Brain Pathol*
1066 **3**, 381-393 (1993).
1067 139. M. Kiessling *et al.*, Differential transcription and translation of immediate early genes in the
1068 gerbil hippocampus after transient global ischemia. *J Cereb Blood Flow Metab* **13**, 914-924
1069 (1993).
1070 140. B. S. Meldrum, Concept of activity-induced cell death in epilepsy: historical and
1071 contemporary perspectives. *Prog Brain Res* **135**, 3-11 (2002).

141. M. Simonato *et al.*, Differential expression of immediate early genes in the hippocampus in the kindling model of epilepsy. *Brain Res Mol Brain Res* **11**, 115-124 (1991).

142. X. Wang, X. Song, L. Wu, J. V. Nadler, R. Z. Zhan, Persistent Hyperactivity of Hippocampal Dentate Interneurons After a Silent Period in the Rat Pilocarpine Model of Epilepsy. *Front Cell Neurosci* **10**, 94 (2016).

143. G. Feng *et al.*, Imaging neuronal subsets in transgenic mice expressing multiple spectral variants of GFP. *Neuron* **28**, 41-51 (2000).

144. G. Zhang, Z. Gao, S. Guan, Y. Zhu, J. H. Wang, Upregulation of excitatory neurons and downregulation of inhibitory neurons in barrel cortex are associated with loss of whisker inputs. *Mol Brain* **6**, 2 (2013).

145. G. Paxinos, C. Watson, *The Mouse Brain: in stereotaxic coordinates*. G. Paxinos, C. Watson, Eds., The Rat Brain: in stereotaxic coordinates (Elsevier Academic Press, 2005).

1086 **Figures and legends**

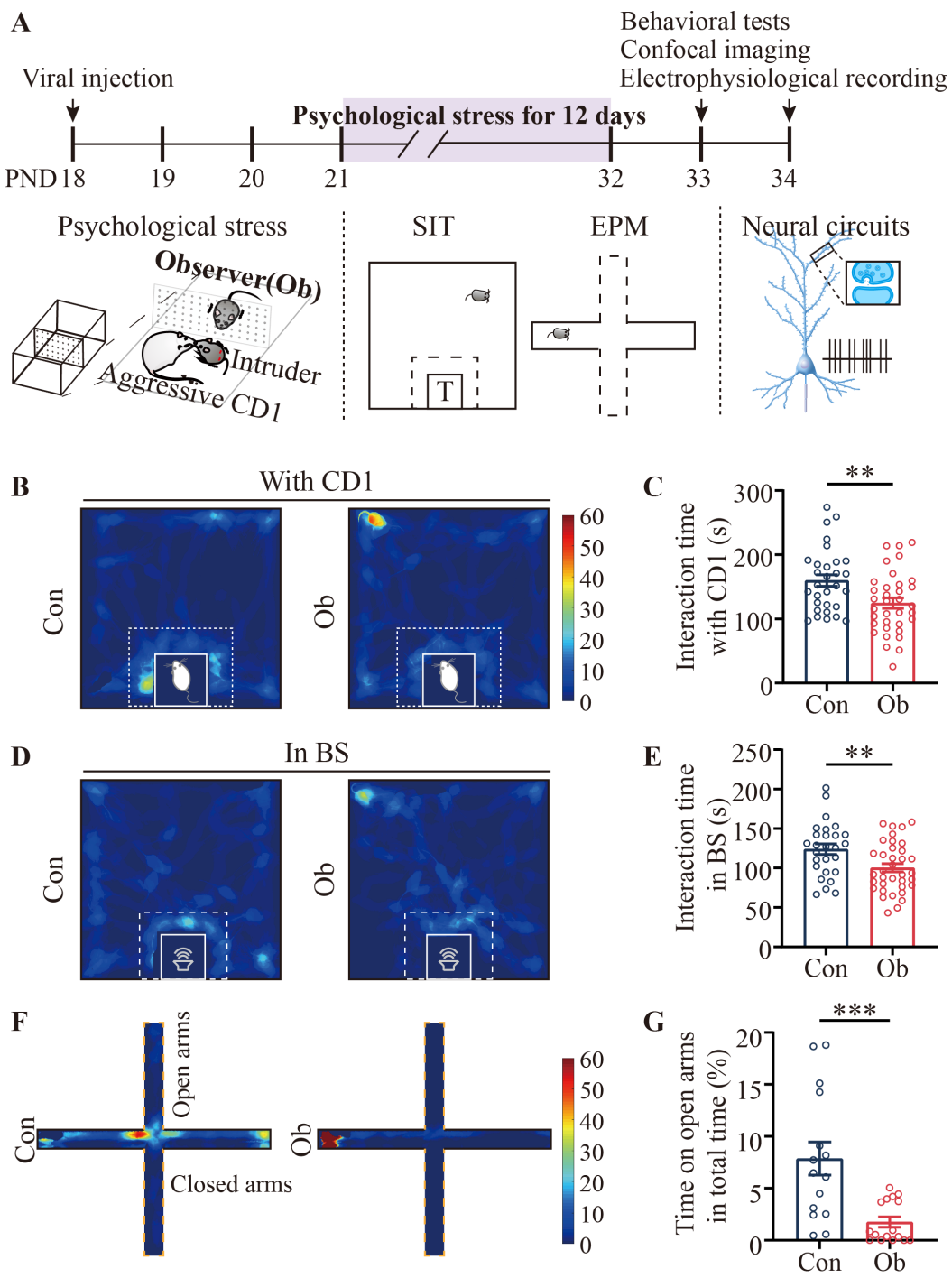

1087

1088 **Figure 1. Psychological stress induces fear memory and anxiety-like behavior in mice. A)** Experiment
1089 timeline and diagrams for mice to witness resident/intruder paradigm and to be examined by social
1090 interaction test, elevated-plus maze test and cellular plasticity. **B)** Heat maps illustrate the social
1091 interaction test for C57 control (Con) and observational (Ob) mice in face to a CD1 resident mouse. **C)**
1092 A bar graph with samples' dots show the interaction time of C57 mice with CD1 resident. **D)** Heat

maps illustrate the social interaction test for C57 mice in response to battle sound. **E)** A bar graph with samples' dots shows the interaction time of C57 mice with the battle sound. **F)** Heat maps illustrate the elevated-plus maze test for control and observational mice. **G)** A bar graph with sample dots shows the time spent on open arms in the total time on the elevated-plus maze. Abbreviations: PND, postnatal day; SIT, social interaction test; EPM, elevated plus maze; Ob, observer; Con, control; BS, battle sound. Data are presented as mean ± SEM and analyzed by one-Way ANOVA. Three asterisks, $p<0.001$; two asterisks, $p<0.01$.

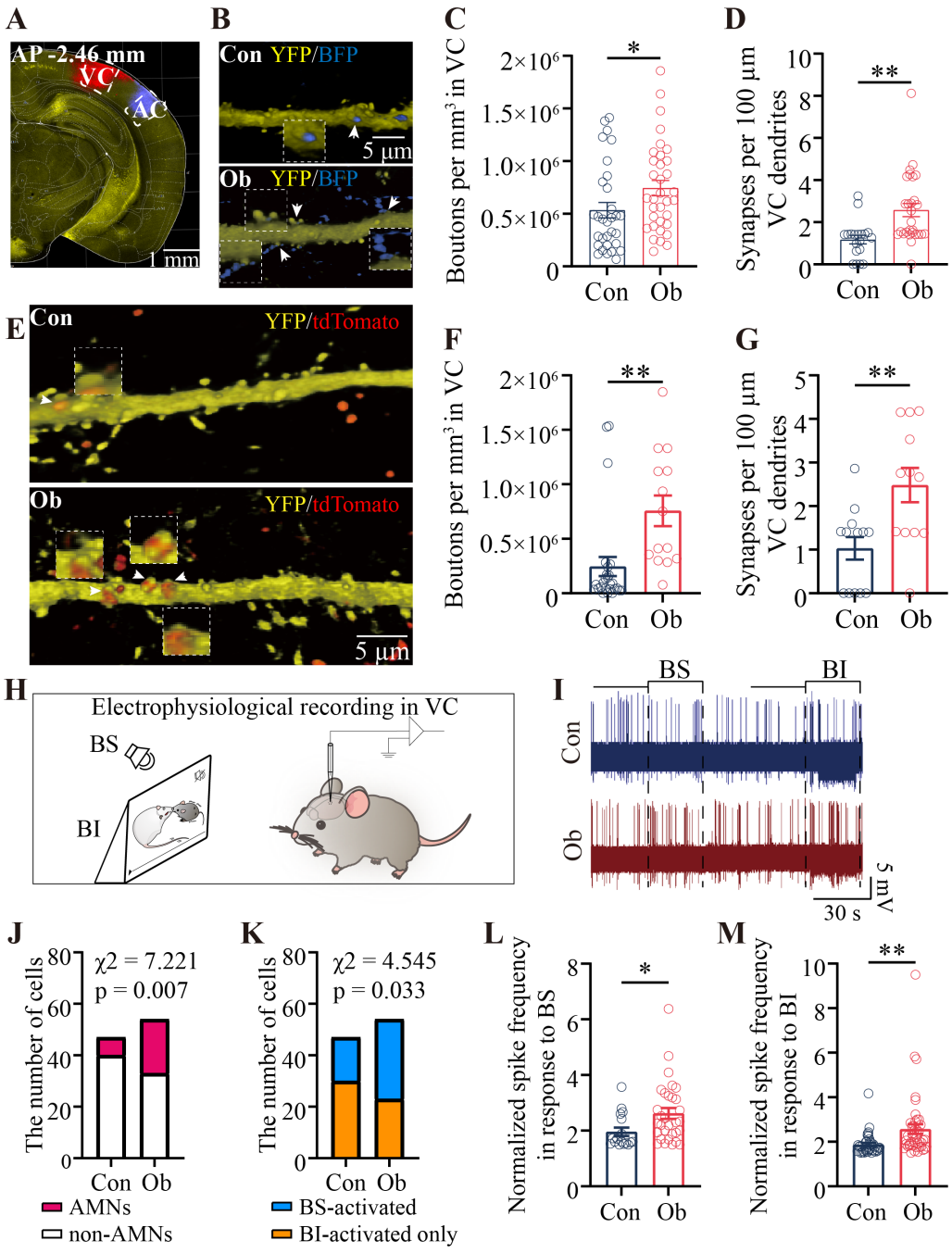

Figure 2. Psychological stress elevates the number of synaptic contacts and associative memory neurons in the VC. A) Confocal image illustrates the injection sites of AAV2/8-CMV-BFP in AC and AAV2/8-CMV-tdTomato in VC. **B)** BFP-labeled AC axonal boutons and their contacts on YFP-labeled dendritic spines of VC neurons from Con mouse (top panel) and Ob mouse (bottom panel). Images in white dash-line boxes show the amplification of synaptic contacts (1.68X) pointed by white arrows that denote synaptic contacts. **C)** The statistical analyses of axon boutons per mm^3 in the VC projected from the AC in Con and Ob mice (one-way ANOVA). **D)** The statistical analyses of synaptic contacts per

100 μm dendrite made between AC axon boutons and dendritic spines on VC neurons (one-way ANOVA). **E)** RFP-labeled VC axonal boutons and their contacts on YFP-labeled dendritic spines of VC neurons from Con mouse (top panel) and Ob mouse (bottom panel). Images in white dash-line boxes show the amplification of synaptic contacts (2.0X) pointed by white arrows that denote synaptic contacts. **F)** The statistical analyses of axon boutons per mm^3 in the VC projected from the VC in Con and Ob mice (one-way ANOVA). **G)** The statistical analyses of synaptic contacts per 100 μm dendrite made between VC axon boutons and dendritic spines on VC neurons. **H)** A scheme shows *in vivo* electrophysiological recordings in VC as well as stimulations by battle image (BI) and battle sound (BS). **I)** The spikes at VC neurons spontaneously and evoked by BS and BI from Con mouse (blue) and Ob mouse (red). **J)** The statistical analyses about the numbers of associative memory neurons (AMNs, red in bar) that encode both BI and BS as well as of active neurons that encode either BI or BS (non-AMNs, white in bar) in the visual cortex from Con and Ob mice (chi-square test). **K)** The statistical analyses about the numbers of BS-activated neurons (blue in bar) and BI-activated neurons (orange in bar) in the visual cortex from Con and Ob mice (chi-square test). **L)** The statistical analyses about normalized spike frequencies in response to BS in VC neurons from Con and Ob mice (one-way ANOVA). **M)** The statistical analyses about normalized spike frequencies in response to BI in VC neurons from Con and Ob mice (one-way ANOVA). Abbreviations: AP: Anteroposterior; VC, visual cortex; AC, auditory cortex; BS: battle sound; BI: battle image. Data are presented as mean ± SEM. Two asterisks, $p < 0.01$; one asterisk, $p < 0.05$.

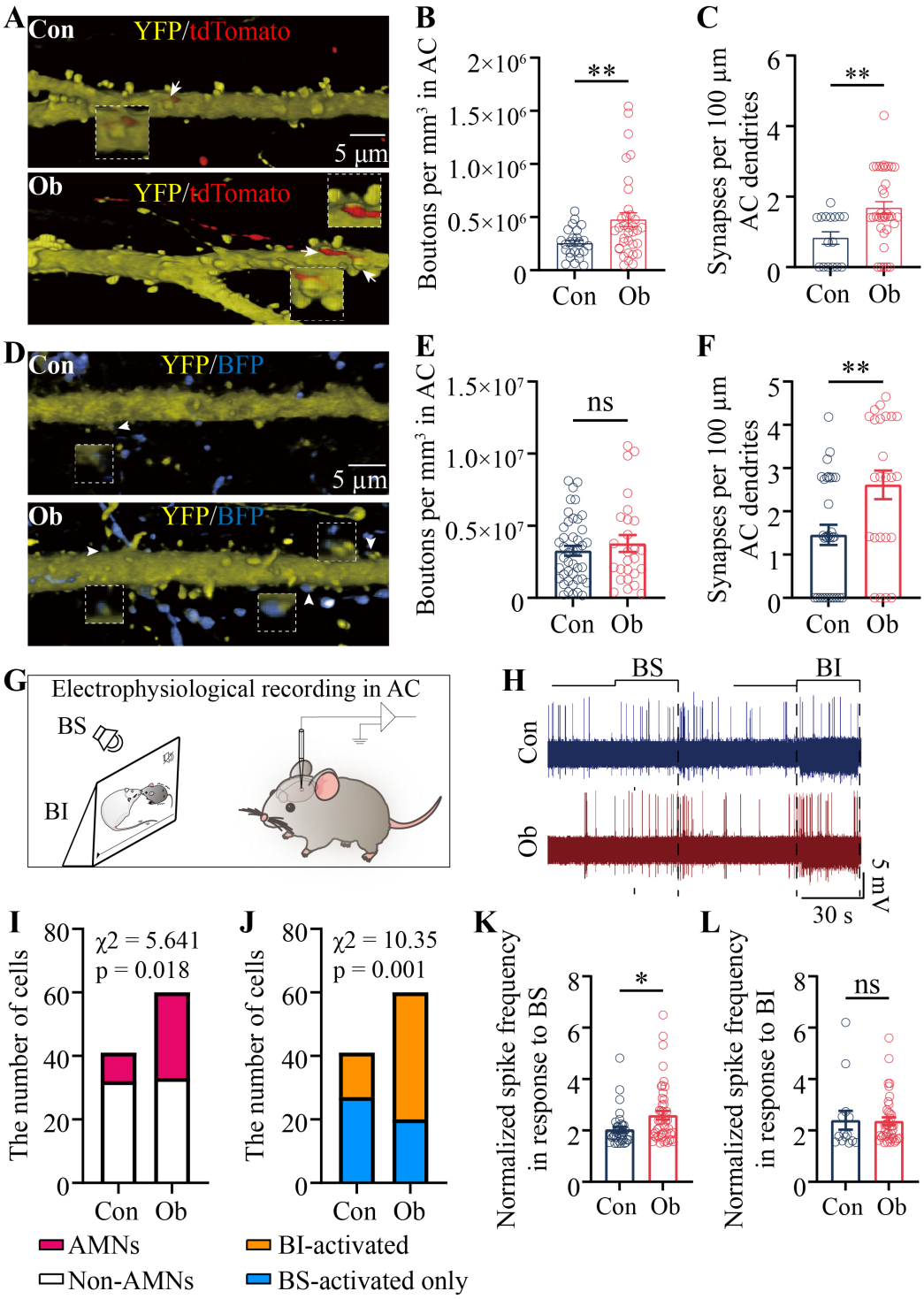

Figure 3. Psychological stress elevates the number of synaptic contacts and associative memory neurons in the AC. A) RFP-labeled VC axon boutons and their contacts on YFP-labeled dendritic spines of AC neurons from Con mouse (top panel) and Ob mouse (bottom panel). Images in white dash-line boxes show the amplification of synaptic contacts (1.68X) pointed by white arrows that denote synaptic contacts. **B)** The statistical analyses of axon boutons per mm^3 in the AC projected from the VC

in Con and Ob mice (one-way ANOVA). **C)** The statistical analyses of synaptic contacts per 100 μm dendrite made between VC axon boutons and dendritic spines on AC neurons (one-way ANOVA). **D)** BFP-labeled AC axon boutons and their contacts on YFP-labeled dendritic spines of AC neurons from Con mouse (top panel) and Ob mouse (bottom panel). Images in white dash-line boxes show the amplification of synaptic contacts (2.0X) pointed by white arrows that denote synaptic contacts. **E)** The statistical analyses of axon boutons per mm^3 in the AC projected from the AC in Con and Ob mice (one-way ANOVA). **F)** The statistical analyses of synaptic contacts per 100 μm dendrite made between AC axon boutons and dendritic spines on AC neurons. **G)** A scheme shows *in vivo* electrophysiological recordings in AC as well as stimulations by battle image (BI) and battle sound (BS). **H)** The spikes at AC neurons spontaneously and evoked by BS and BI from Con mouse (blue) and Ob mouse (red). **I)** The statistical analyses about the numbers of associative memory neurons (AMNs, red in bar) that encode both BI and BS as well as of active neurons that encode either BI or BS (non-AMNs, white in bar) in the auditory cortex from Con and Ob mice (chi-square test). **J)** The statistical analyses about the numbers of BI-activated neurons (orange in bar) and BS-activated neurons (blue in bar) in the auditory cortex from Con and Ob mice (chi-square test). **K)** The statistical analyses about normalized spike frequencies in response to BS in AC neurons from Con and Ob mice (one-way ANOVA). **L)** The statistical analyses about normalized spike frequencies in response to BI in AC neurons from Con and Ob mice (one-way ANOVA). Abbreviations: AP: Anteroposterior; VC, visual cortex; AC, auditory cortex; BS: battle sound; BI: battle image. Data are presented as mean ± SEM. Two asterisks, $p < 0.01$; one asterisk, $p < 0.05$; ns, $p > 0.05$.

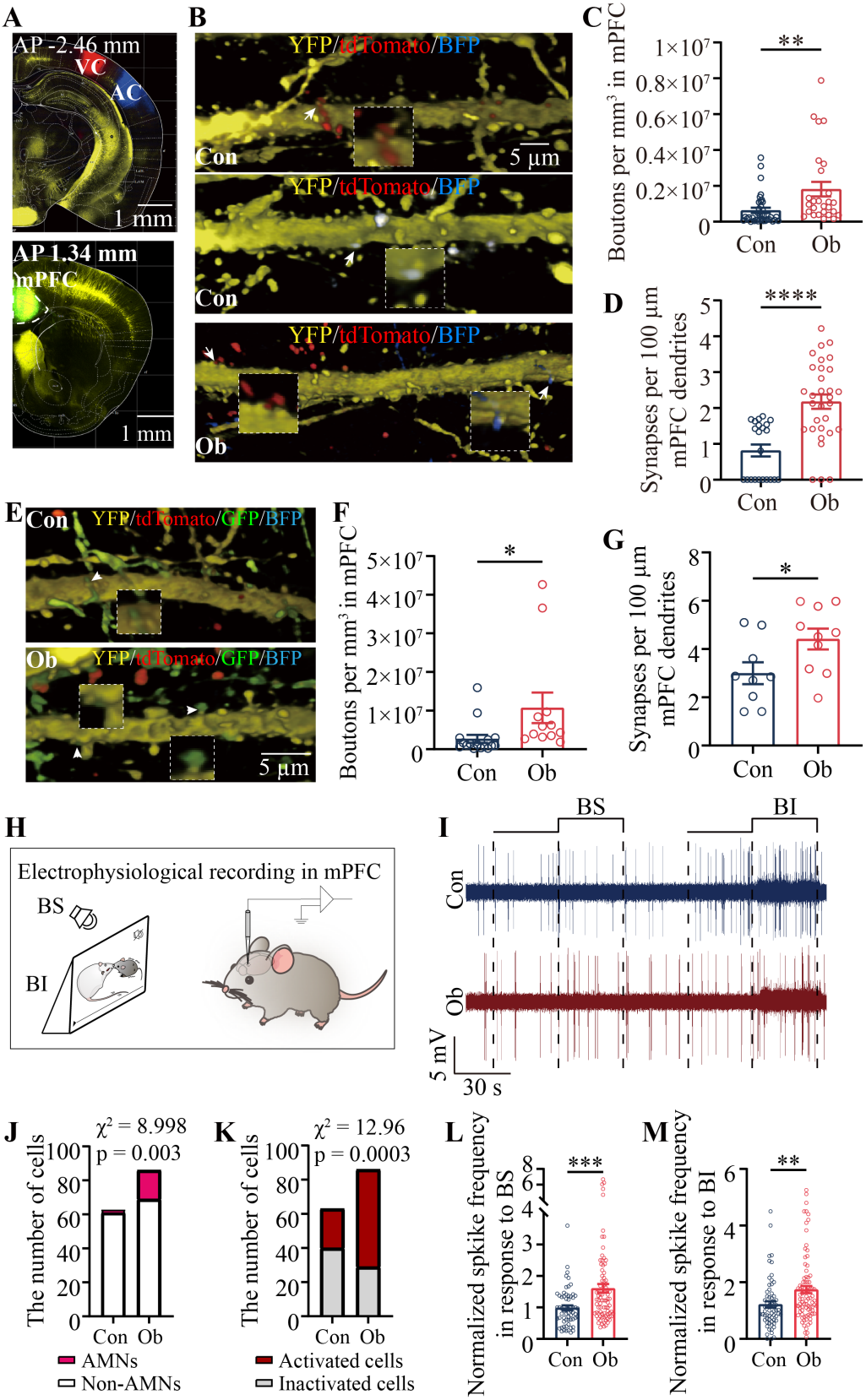

Figure 4. Psychological stress elevates the number of synaptic contacts and associative memory neurons in the mPFC. A) Confocal image demonstrates the injection sites of AAV2/8-CMV-BFP in the

AC, AAV2/8- CMV-tdTomato in the VC (top panel) and AAV2/8-CMV-GFP in mPFC (bottom panel). **B)** RFP-labeled VC axon boutons, BFP-labeled AC boutons and their contacts on YFP-labeled dendritic spines of mPFC neurons from Con mouse (top panel and middle panel) and Ob mouse (bottom panel). Images in white dash-line boxes show the amplification of synaptic contacts (2.0X) pointed by white arrows that denote synaptic contacts. **C)** The statistical analyses of axon boutons per mm^3 in the mPFC projected from the AC and VC in Con and Ob mice (one-way ANOVA). **D)** The statistical analyses of synaptic contacts per 100 μm dendrite made among AC/VC axon boutons and dendritic spines on mPFC neurons (one-way ANOVA). **E)** GFP-labeled mPFC axon boutons and their contacts on YFP-labeled dendritic spines of mPFC neurons from Con mouse (top panel) and Ob mouse (bottom panel). Images in white dash-line boxes show the amplification of synaptic contacts (2.0X) pointed by white arrows that denote synaptic contacts. **F)** The statistical analyses of axon boutons per mm^3 in the mPFC projected from the mPFC in Con and Ob mice (one-way ANOVA). **G)** The statistical analyses of synaptic contacts per 100 μm dendrite made between mPFC axon boutons and dendritic spines on mPFC neurons. **H)** A scheme shows *in vivo* electrophysiological recordings in mPFC as well as stimulations by battle image (BI) and battle sound (BS). **I)** The spikes at mPFC neurons spontaneously and evoked by BS and BI from Con mouse (blue) and Ob mouse (red). **J)** The statistical analyses about the numbers of associative memory neurons (AMNs, red in bar) that encode both BI and BS as well as of non-associative memory neurons (non-AMNs, white in bar) that encode BI, BS or neither signals in the mPFC from Con and Ob mice (chi-square test). **K)** The statistical analyses about the numbers of activated neurons (red in bar) and inactivated neurons that encode neither BI nor BS (grey in bar) in the mPFC from Con and Ob mice (chi-square test). **L)** The statistical analyses about normalized spike frequencies in response to BS in mPFC neurons from Con and Ob mice (one-way ANOVA). **M)** The statistical analyses about normalized spike frequencies in response to BI in mPFC neurons from Con and Ob mice (one-way ANOVA). Abbreviations: AP: Anteroposterior; mPFC: medial prefrontal cortex; VC, visual cortex; AC, auditory cortex; BS: battle sound; BI: battle image. Data are presented as mean ± SEM. Four asterisks, $p < 0.0001$; three asterisks, $p < 0.001$; two asterisks, $p < 0.01$; one asterisk, $p < 0.05$.

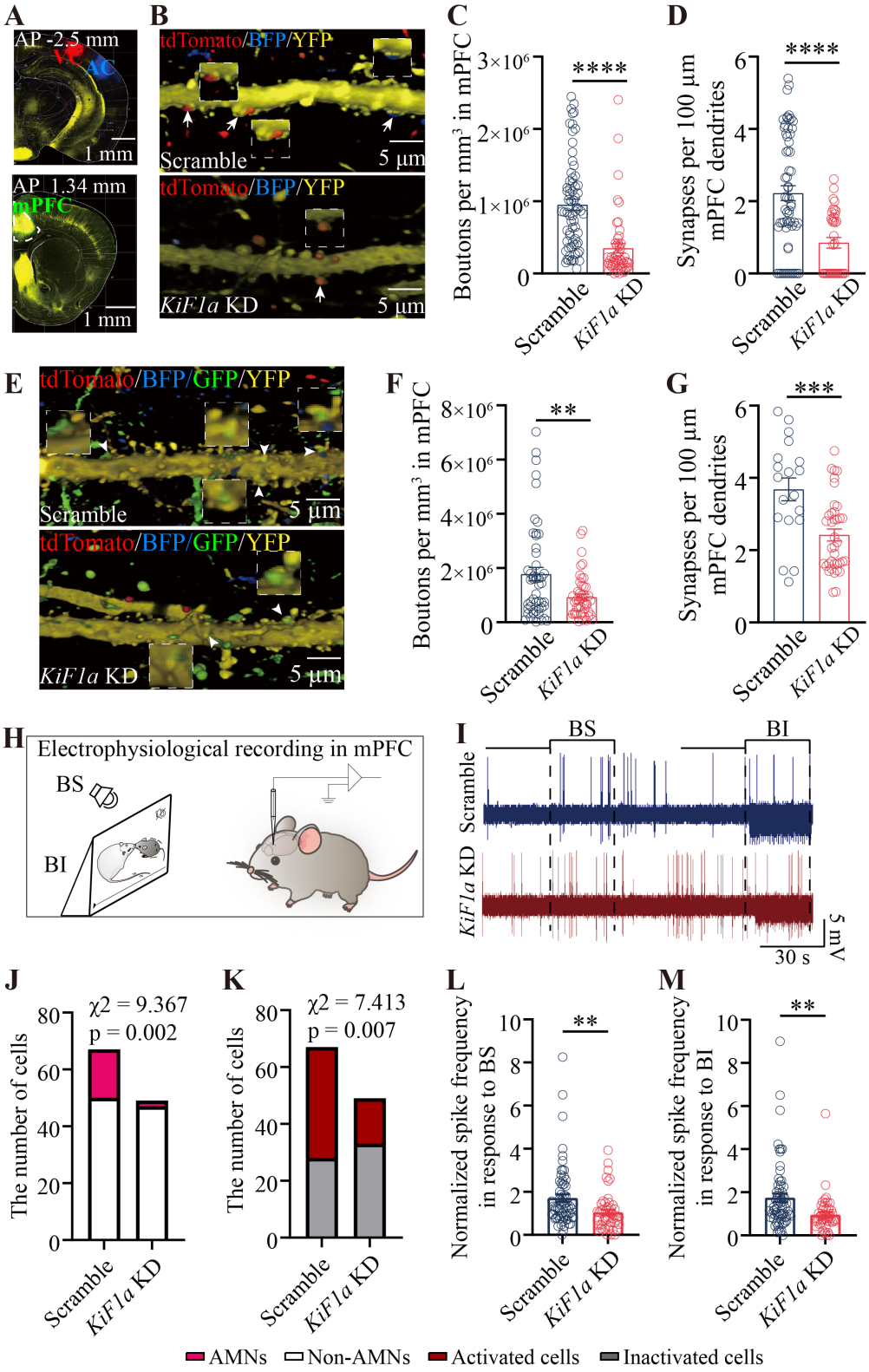

1187

1188 **Figure 5. *KiF1a* RNAi in mPFC precludes the stress-induced recruitments of axon projection, synapse**

1189 **formation and associative memory neurons. A)** Confocal image illustrates the injection sites of

1190 AAV2/8-CMV-BFP in AC, AAV2/8-CMV-tdTomato in VC (top panel) and AAV2/9-U6-shRNA-GFP in mPFC

1191 (bottom panel). **B)** RFP-labeled VC axon boutons, BFP-labeled AC boutons and their contacts on
1192 YFP-labeled dendritic spines of mPFC neurons from scramble mouse (top panel) and *KiF1a*-KD mouse
1193 (bottom panel). Images in white dash-line boxes show the amplification of synaptic contacts (1.2X)
1194 pointed by white arrows that denote synaptic contacts. **C)** The statistical analyses of axon boutons per
1195 mm^3 in the mPFC projected from the AC and VC in scramble and *KiF1a*-KD mice (one-way ANOVA). **D)**
1196 The statistical analyses of synaptic contacts per 100 μm dendrite made among AC, VC axon boutons
1197 and dendritic spines on mPFC neurons (one-way ANOVA). **E)** GFP-labeled mPFC axon boutons and
1198 their contacts on YFP-labeled dendritic spines of mPFC neurons from scramble mouse (top panel) and
1199 *KiF1a*-KD mouse (bottom panel). Images in white dash-line boxes show the amplification of synaptic
1200 contacts (2.3X) pointed by white arrows that denote synaptic contacts. **F)** The statistical analyses of
1201 axon boutons per mm^3 in the mPFC projected from the mPFC in scramble and *KiF1a*-KD mice (one-way
1202 ANOVA). **G)** The statistical analyses of synaptic contacts per 100 μm dendrite made between mPFC
1203 axon boutons and dendritic spines on mPFC neurons. **H)** A scheme shows *in vivo* electrophysiological
1204 recordings in mPFC as well as stimulations by battle image (BI) and battle sound (BS). **I)** The spikes at
1205 mPFC neurons spontaneously and evoked by BS and BI from scramble mouse (blue) and *KiF1a*-KD
1206 mouse (red). **J)** The statistical analyses about the numbers of associative memory neurons (AMNs, red
1207 in bar) that encode both BI and BS as well as of non-associative memory neurons (non-AMNs, white in
1208 bar) that encode BI, BS or neither signals in the mPFC cortex from scramble and *KiF1a*-KD mice
1209 (chi-square test). **K)** The statistical analyses about the numbers of active neurons (red in bar) and
1210 inactive neurons that encode neither BI nor BS (grey in bar) in the mPFC cortex from scramble and
1211 *KiF1a*-KD mice (chi-square test). **L)** The statistical analyses about normalized spike frequencies in
1212 response to BS in mPFC neurons from scramble and *KiF1a*-KD mice (one-way ANOVA). **M)** The
1213 statistical analyses about normalized spike frequencies in response to BI in mPFC neurons from
1214 scramble and *KiF1a*-KD mice (one-way ANOVA). Abbreviations: AP: Anteroposterior; mPFC: medial
1215 prefrontal cortex; VC, visual cortex; AC, auditory cortex; BS: battle sound; BI: battle image. Data are
1216 presented as mean ± SEM. our asterisks, $p < 0.0001$; three asterisks, $p < 0.001$; two asterisks, $p < 0.01$.

1217

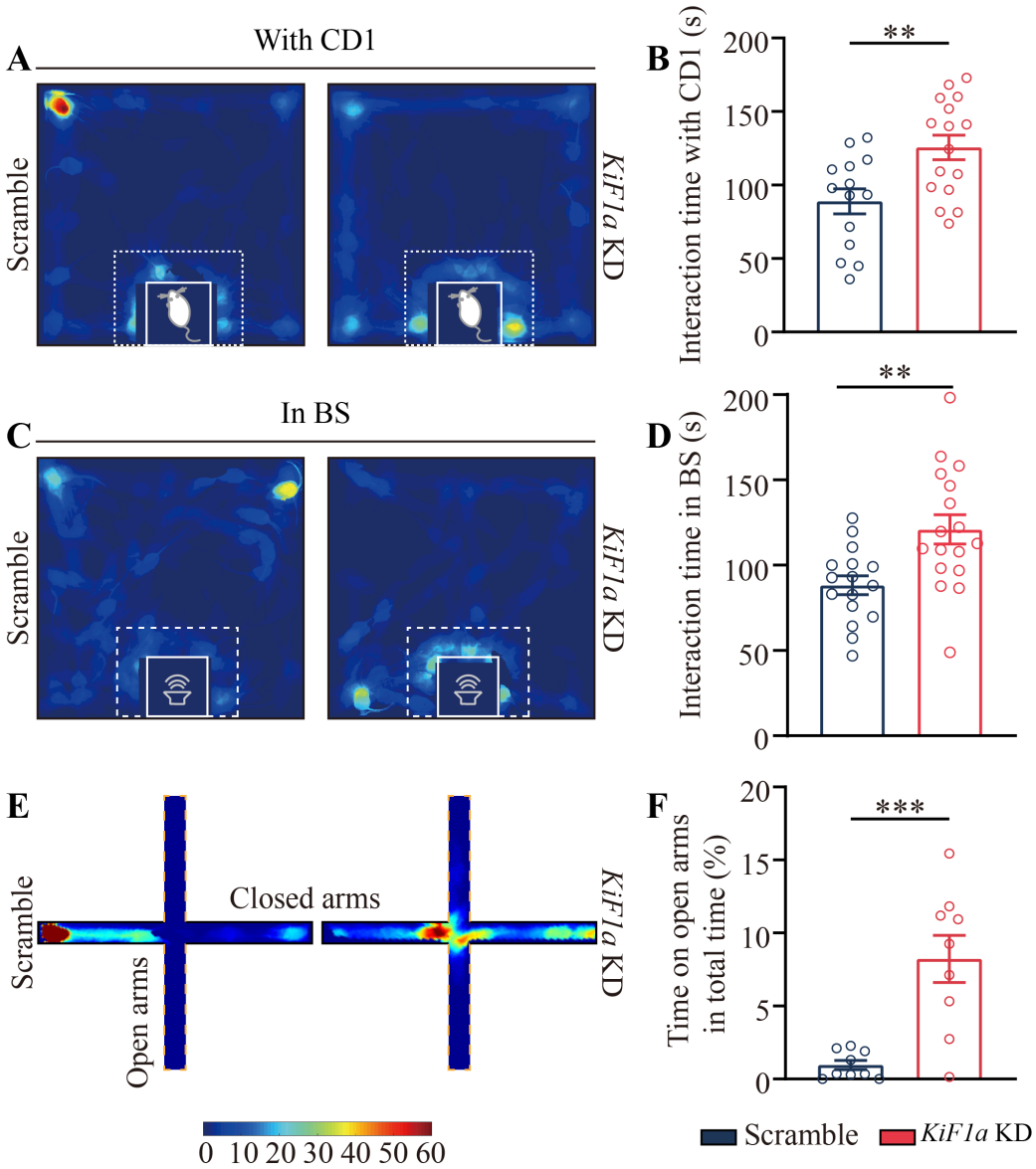

Figure 6. *KiF1a* RNAi in mPFC attenuates stress-induced fear memory and anxiety-like behavior. A) Heat maps illustrate the social interaction test for C57 scramble and *KiF1a*-KD mice in face to a CD1 resident mouse. **B)** A bar graph with samples' dots shows the interaction time of Ob plus *KiF1a*-KD and scramble mice with CD1 resident. **C)** Heat maps show the social interaction test for Ob plus *KiF1a*-KD and scramble mice in response to battle sound. **D)** A bar graph with samples' dots shows the interaction time of Ob plus *KiF1a*-KD and scramble mice with battle sound. **E)** Heat maps illustrate the elevated-plus maze test for Ob plus scramble and *KiF1a* KD mice. **F)** A bar graph with samples' dots for show the time spent on open arms in the total time on the elevated-plus maze. Abbreviations: KD: knock down; BS, battle sound. Data are presented as mean ± SEM and analyzed by one-Way ANOVA. Three asterisks, p<0.001; two asterisks, p<0.01

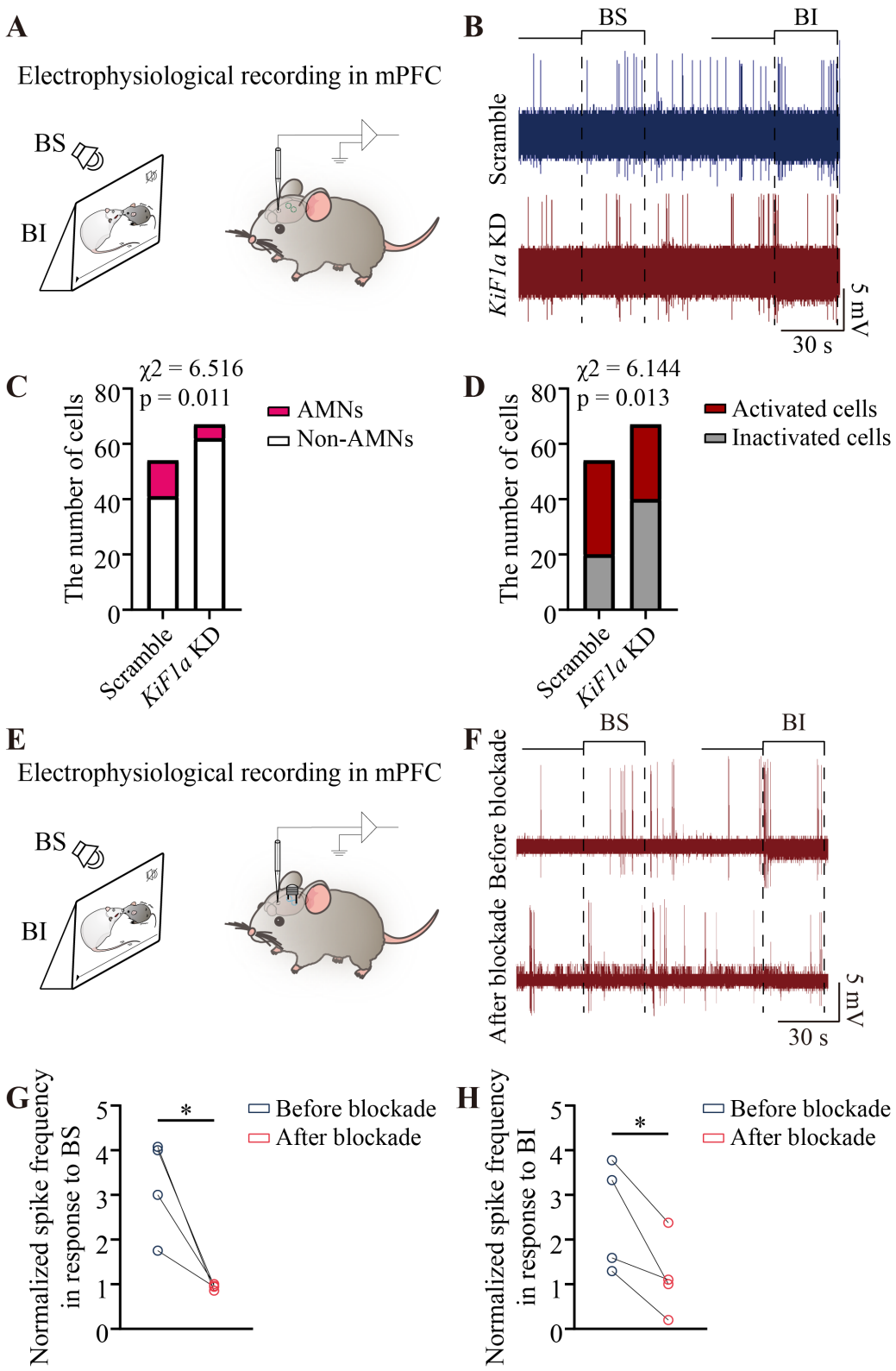

Figure 7 The inhibition of VC and AC neurons impairs the activity of associative memory neurons in mPFC. A) A scheme shows *in vivo* electrophysiological recordings in the mPFC and the stimulations of

battle sound (BS) and battle image (BI). Green dashed circles on the tope of mouse head show AAV-shRNA (scramble) or AAV-sh*KiF1a* are simultaneously injected into VC and AC. **B)** The spikes at mPFC associative memory neurons spontaneously and evoked by BS and BI from scramble mouse (blue) and *KiF1a*-KD mouse (red). **C)** The statistical analyses about the numbers of associative memory neurons (AMNs, red in bar) that encode both BI and BS as well as of non-associative memory neurons (non-AMNs, white in bar) that encode BI, BS or neither signals in the mPFC from scramble and *KiF1a*-KD mice (chi-square test). **D)** The statistical analyses about the numbers of active neurons (red in bar) and inactive neurons that encode neither BI nor BS (grey in bar) in the mPFC from scramble and *KiF1a*-KD mice (chi-square test). **E)** A diagram shows *in vivo* electrophysiological recordings in the mPFC and stimulations of battle sound (BS) and battle image (BI). Blue dashed circles on the top of mouse head show VC and AC blockade by CNQX and DAP5. **F)** The spikes at mPFC associative memory neurons spontaneously and evoked by BS and BI before and after AC and VC blockade. **G)** The statistical analyses about normalized spike frequencies in response to BS in mPFC associative memory neurons before and after AC and VC blockade (paired *t*-test). **H)** The statistical analyses about normalized spike frequencies in response to BI in mPFC associative memory neurons before and after AC and blockade (paired *t*-test). Abbreviation: KD: knock down; BS: battle sound; BI: battle image. One asterisk, $p < 0.05$.

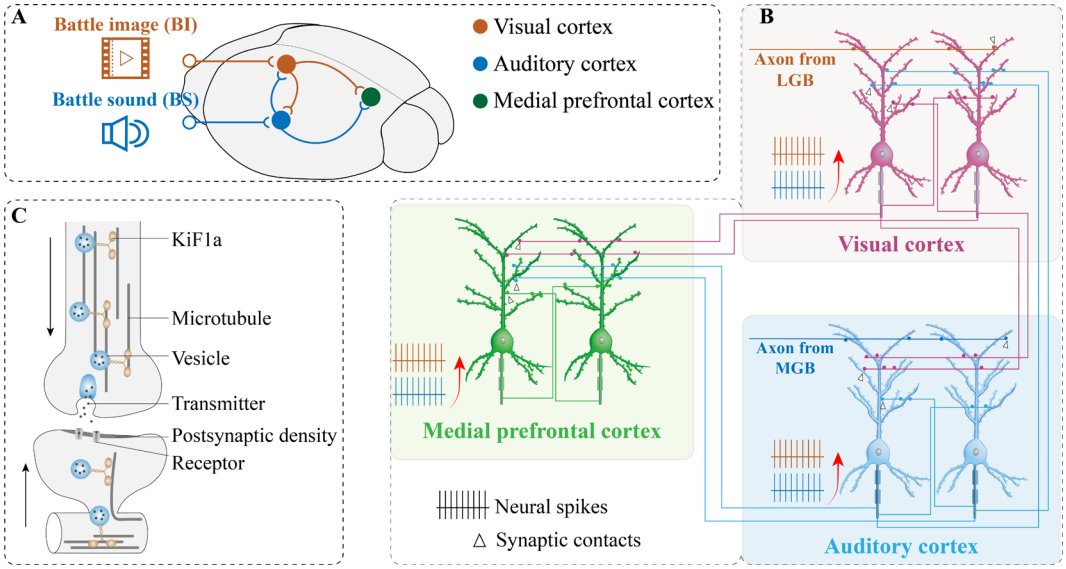

Figure 8 Cellular infrastructure in the auditory cortex, visual cortex and the medial prefrontal cortex correlated to the fear induced by psychological stress. A) The stressful signals, in which battle images (BI) are inputted to the visual cortex (VC) and battle sounds (BS) are inputted to the auditory cortex (AC), induce the synapse interconnections between auditory and visual cortical neurons as well as the convergent synapse innervations onto the neurons in the medial prefrontal cortex (mPFC) in the mice of witnessing the resident/intruder paradigm. **B)** Battle images (BI) are transmitted to the visual cortex via the axons of the lateral geniculate body (LGB). Battle sounds are transmitted to the auditory cortex via the axons of the medial geniculate body (MGB). The neurons in the visual cortex and the auditory cortex are interconnected through *en passant* synapses, or the contacts between presynaptic boutons and postsynaptic spines, after their coactivity, such that they encode battle images and battle sound, i.e., they are recruited as the primary associative memory neurons (pAMN). The neurons in the medial prefrontal cortex (mPFC) receive the convergent synapse innervations from the VC and the AC after their coactivity, such that they encode battle images and battle sound, i.e., they are recruited as the secondary associative memory neurons (sAMN). In the meantime, the intramodal interconnections via collateral axons and *en passant* synapses are strengthened among the neurons within the VC, the AC and the mPFC. After associative memory neurons are recruited, their activity strength is upregulated. **C)** KIF1A in axons and dendrites fulfills the intracellular transportations of synaptic vesicles, receptors and synapse-building elements to coordinate the axon projection, spine expansion and new synapse formation, which are essential for fear memory and anxiety-like behaviors induced by psychological traumas.

Supplemental figures and legends:

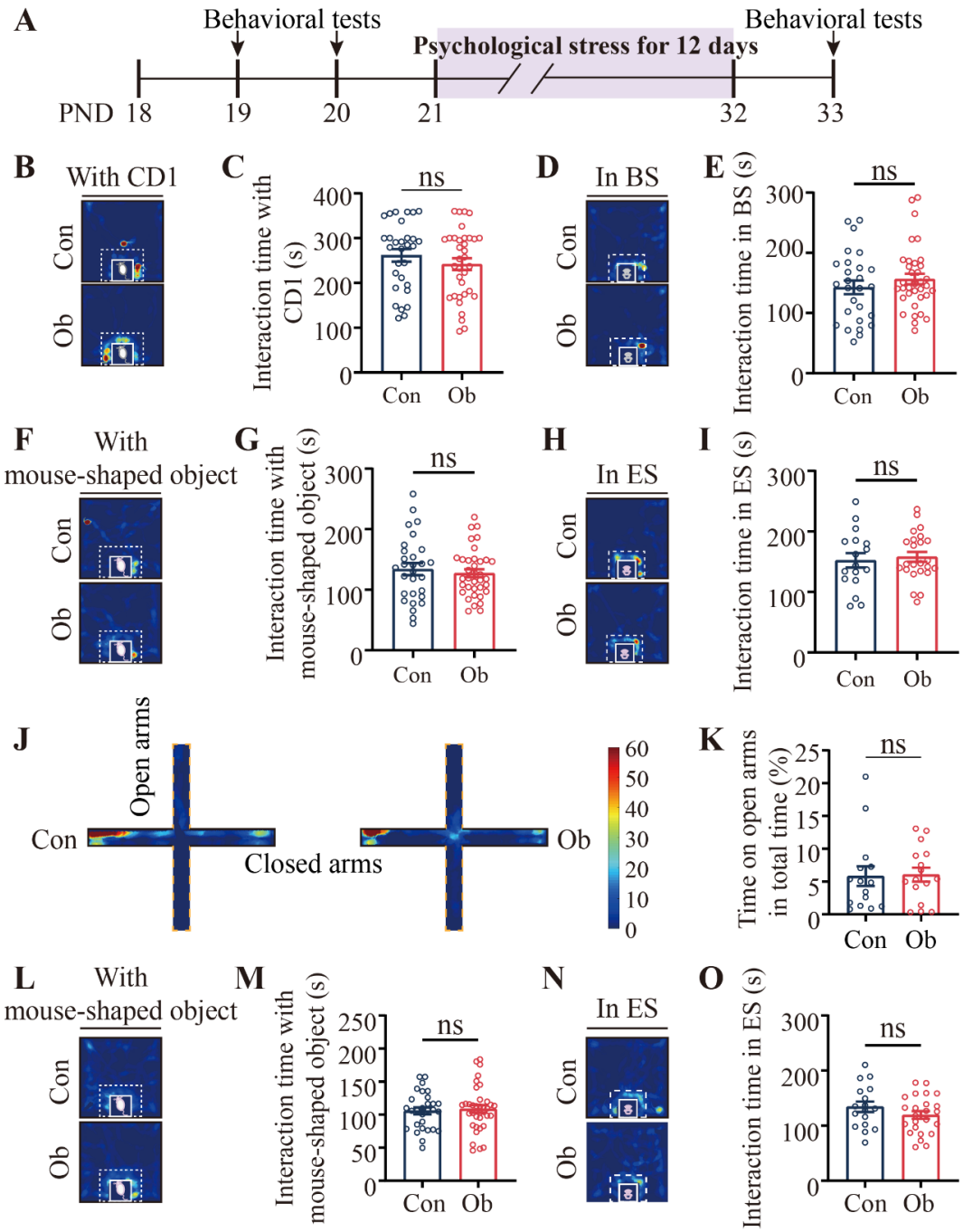

Extended Data Figure 1. Psychological stress promotes fear memory formation specific to trauma-associated contexts in mice. A) Experimental timeline for mice to witness resident/intruder paradigm and to be conducted by social interaction test, elevated-plus maze test. **B)** Heat maps illustrate the social interaction test for C57 control (Con) and observational (Ob) mice in face to a CD1 resident mouse at PND 19. **C)** The bar graph with dots for each of samples show the interaction time of C57 mice with CD1 resident mouse at PND 19. **D)** Heat maps illustrate the social interaction test for C57 mice in response to battle sound at PND 19. **E)** The bar graph with dots for each of examples show the interaction time of C57 mice with the battle sound at PND 19. **F)** Heat maps illustrate the social interaction test for C57 mice in face to an artificial

mouse model at PND 19. **G)** The bar graph with dots for each of samples show the interaction time of C57 mice with artificial mouse model at PND 19. **H)** Heat maps illustrate the social interaction test for C57 mice in response to housing environmental sound at PND 19. **I)** The bar graph with dots for each of examples show the interaction time of C57 mice with the housing environmental sound at PND 19. **J)** Heat maps illustrate the elevated-plus maze test for control and observational mice at PND 20. **K)** The bar graph with dots for each of samples show the time spent on open arms in the total time on the elevated-plus maze at PND 20. **L)** Heat maps illustrate the social interaction test for C57 mice in face to an artificial mouse model at PND 33. **M)** The bar graph with dots for each of samples show the interaction time of C57 mice with artificial mouse model at PND 33. **N)** Heat maps illustrate the social interaction test for C57 mice in response to housing environmental sound at PND 33. **O)** The bar graph with dots for each of examples show the interaction time of C57 mice with the housing environmental sound at PND 33. Abbreviations: PND: postnatal days; BS: battle sound; ES: housing environmental sound. ns means no statistic significant, $p>0.05$.

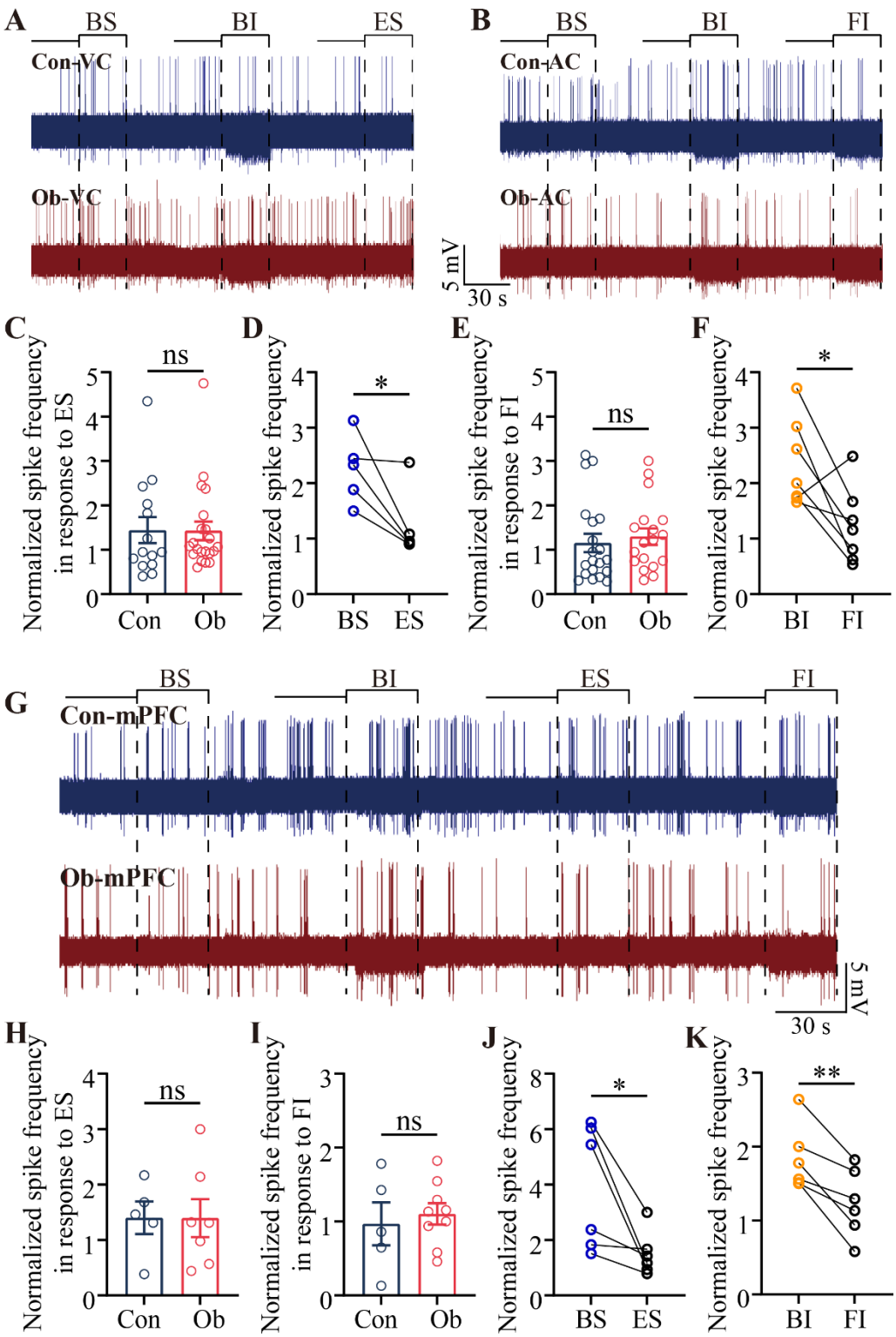

Extended Data Figure 2. Neurons preferentially encode trauma-related information under psychological stress. **A)** The traces of spikes at VC neurons are spontaneously and evoked by BS, BI and ES from Con mouse (blue) and Ob mouse (red). **B)** The traces of spikes at AC neurons are spontaneously and evoked by BS, BI and FI from Con mouse (blue) and Ob mouse (red). **C)** Statistical comparisons about normalized spike frequencies in response to ES in VC neurons from Con and Ob mice (one-way ANOVA). **D)** Statistical comparisons about normalized spike

frequencies in response to BS and ES in VC neurons (paired *t*-test). **E)** Statistical comparisons about normalized spike frequencies in response to FI in AC neurons from Con and Ob mice (one-way ANOVA). **F)** Statistical comparisons about normalized spike frequencies in response to BI and FI in AC neurons (paired *t*-test). **G)** The traces of spikes at mPFC neurons spontaneously and evoked by BS, BI, ES and FI from Con mouse (blue) and Ob mouse (red). **H)** Statistical comparisons about normalized spike frequencies in response to ES in mPFC neurons from Con and Ob mice (one-way ANOVA). **I)** Statistical comparisons about normalized spike frequencies in response to FI in mPFC neurons from Con and Ob mice (one-way ANOVA). **J)** Statistical comparisons about normalized spike frequencies in response to BS and ES in mPFC neurons (paired *t*-test) **K)** Statistical comparisons about normalized spike frequencies in response to BI and FI in mPFC neurons (paired *t*-test). Abbreviations: PND: postnatal days; BS: battle sound; ES: housing environmental sound; BI: battle image; FI: flower image. Two asterisks, $p < 0.01$; one asterisk, $p < 0.05$; ns, $p > 0.05$.

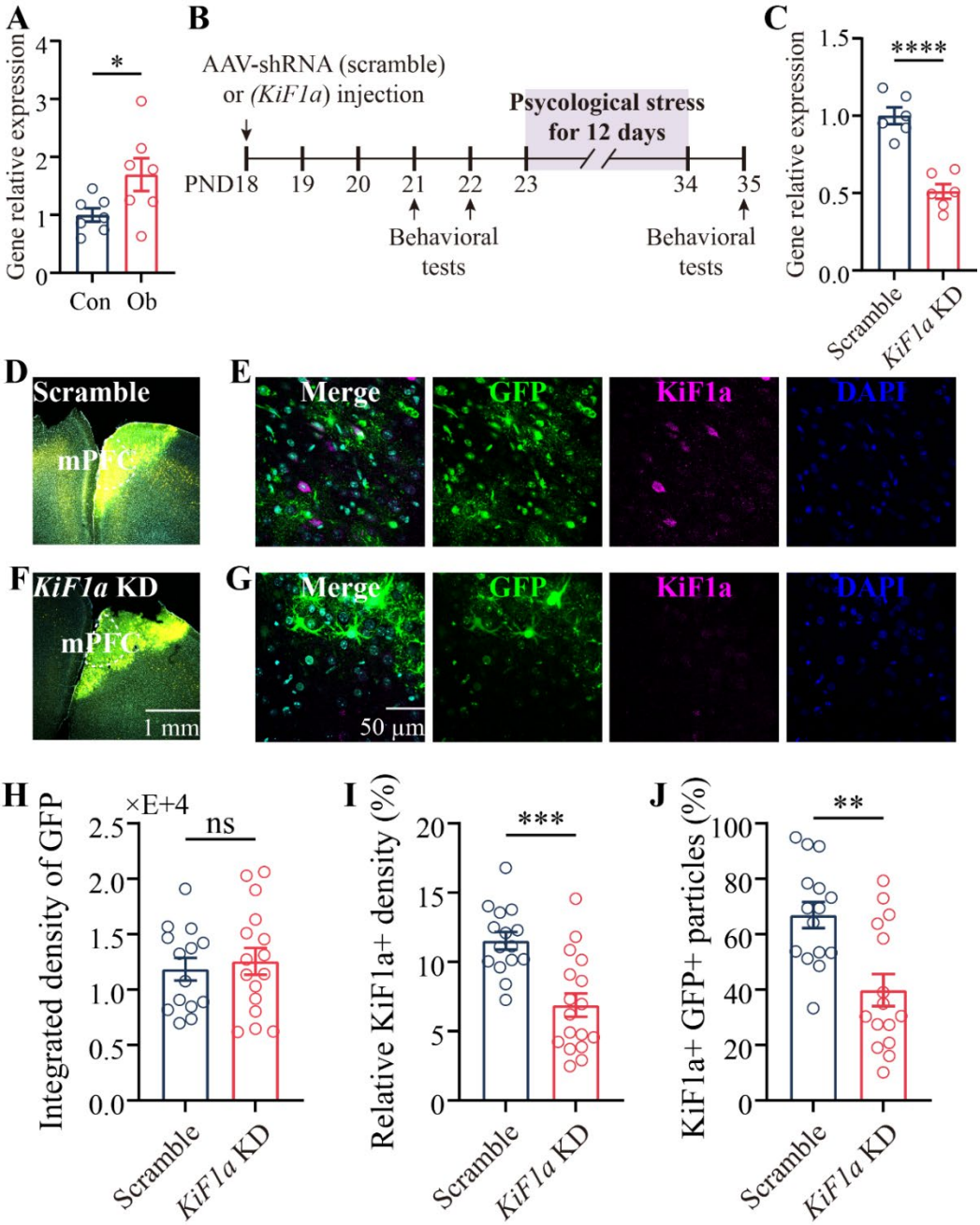

Extended Data Figure 3. Psychological stress upregulates *KiF1a* expression in the mPFC and is suppressed by AAV-sh*KiF1a*-GFP knockdown. A) *KiF1a* gene relative expression in mPFC of Con and Ob mice (one-way ANOVA). **B)** Experimental timeline for RNAi performing and behavioral tests. **C)** The transcriptional level of *KiF1a* are analyzed following AAV-mediated knockdown of *KiF1a* (one-way ANOVA). **D)** Confocal image illustrates the injection sites of AAV-shRNA (scramble)-GFP. **E)** Representative confocal images of KiF1a protein level in mPFC of scramble mice. GFP labeled cells are infected with AAV-shRNA (scramble)-GFP. Magenta labeled cells are KiF1a positive cells. DAPI labeled cell nucleus. **F)** Confocal image illustrates the injection sites of AAV-shRNA (*KiF1a*)-GFP. **G)** Representative images of KiF1a protein level in mPFC of knockdown group mice. GFP labeled cells are infected with AAV- shRNA (*KiF1a*)-GFP.

Magenta labeled cells are KiF1a positive cells. DAPI labeled cell nucleus. **H)** Statistic of integrated density of GFP in mPFC of scramble group mice and knockdown group mice (one-way ANOVA). **I)** Statistic of relative density of KiF1a in mPFC of scramble group mice and knockdown group mice. The data are calculated as the fluorescence intensity ratio of KiF1a to DAPI (one-way ANOVA). **J)** Statistic of the number of KiF1a and GFP double-labeled cellular particles in mPFC of scramble group mice and knockdown group mice (one-way ANOVA). The data are calculated as the ratio of KiF1a/GFP double-labeled to GFP-labeled cellular particles. Abbreviations: Con: control; Ob: observer; mPFC: medial prefrontal cortex. All data are shown as mean ± SEM. Four asterisks, $p < 0.0001$; three asterisks, $p < 0.001$; two asterisks, $p < 0.01$; one asterisk, $p < 0.05$; ns, $p > 0.05$.

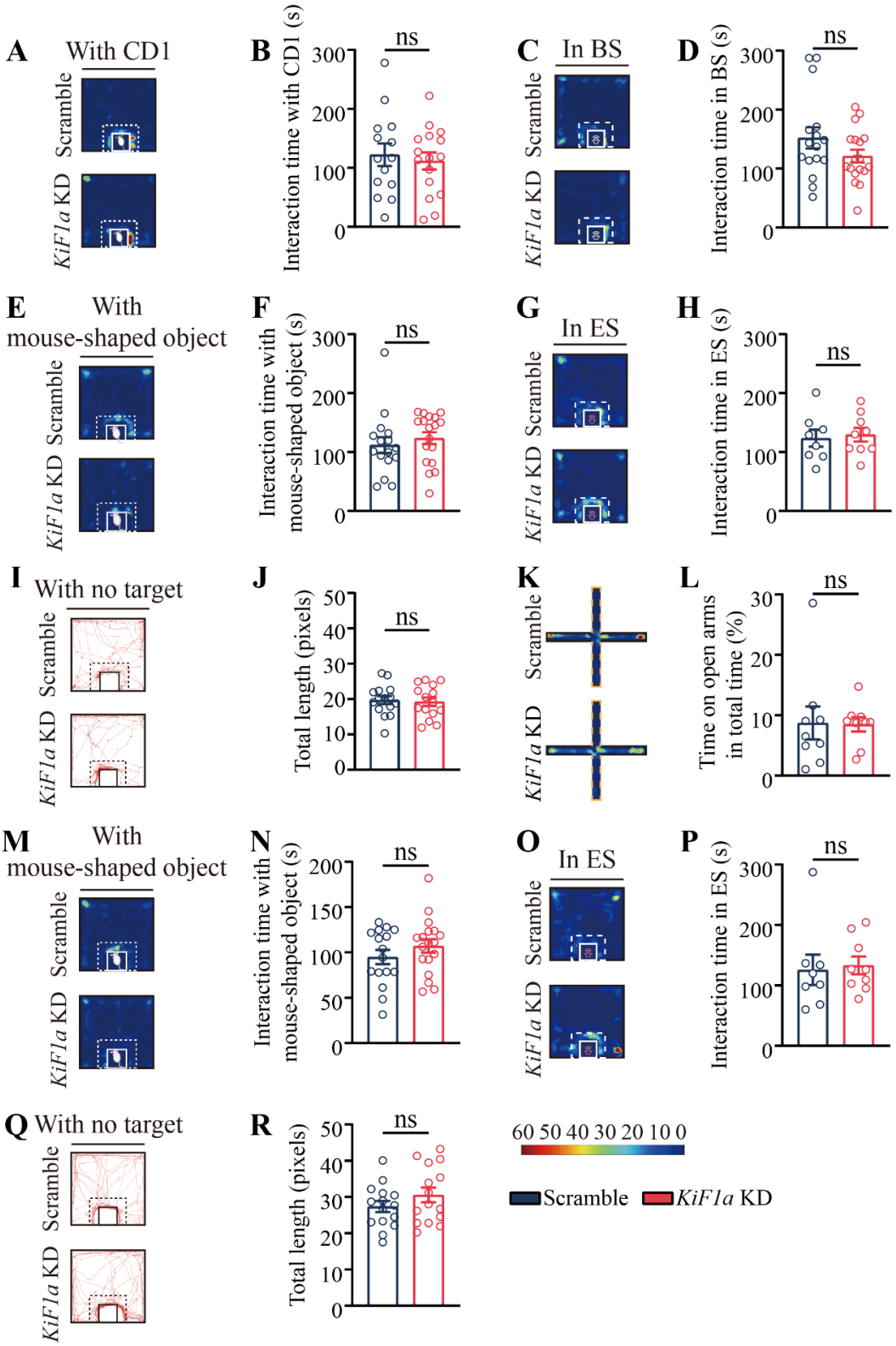

Extended Data Figure 4. KiF1a knockdown does not affect interaction with neutral cues or locomotion. A) Heat maps illustrate the social interaction test for C57 scramble and *KiF1a* KD mice in face to a CD1 resident mouse at PND 21. **B)** The bar graphs with dots for each of samples show the interaction time of C57 mice with CD1 resident mice at PND 21. **C)** Heat maps illustrate

the social interaction test for C57 scramble and *KiF1a* KD mice in response to battle sound at PND 21. **D)** The bar graphs with dots for each of examples show the interaction time of C57 mice with the battle sound at PND 21. **E)** Heat maps illustrate the social interaction test for C57 scramble and *KiF1a* KD mice in face to an artificial mouse model at PND 21. **F)** The bar graphs with dots for each of samples show the interaction time of C57 mice with artificial mouse model at PND 21. **G)** Heat maps illustrate the social interaction test for C57 mice in response to housing environmental sound at PND 21. **H)** The bar graphs with dots for each of examples show the interaction time of C57 mice with the housing environmental sound at PND 21. **I)** Locomotion traces of PND 21 scramble and *KiF1a* KD mice in the social interaction test. **J)** The bar graphs with dots for each of samples show the total movement trajectory length of C57 mice at PND 21. **K)** Heat maps illustrate the elevated-plus maze test for scramble and *KiF1a* KD mice at PND 22. **L)** The bar graphs with dots for each of samples show the time spent on open arms in the total time on the elevated-plus maze at PND 22. **M)** Heat maps illustrate the social interaction test for C57 scramble and *KiF1a* KD mice in face to an artificial mouse model at PND 35. **N)** The bar graphs with dots for each of samples show the interaction time of C57 mice with artificial mouse model at PND 35. **O)** Heat maps illustrate the social interaction test for C57 mice in response to housing environmental sound at PND 35. **P)** The bar graphs with dots for each of examples show the interaction time of C57 mice with the housing environmental sound at PND 35. **Q)** Locomotion traces of PND 35 scramble and *KiF1a* KD mice in the social interaction test. **R)** The bar graphs with dots for each of samples show the total movement trajectory length of C57 mice at PND 35. All data are shown as mean ± SEM and analyzed by one-way ANOVA. Blue symbols show the data of scramble group mice. Red symbols show the data of *KiF1a* KD group mice. Abbreviations: PND: postnatal days; BS: battle sound; ES: housing environmental sound. ns, $p > 0.05$.

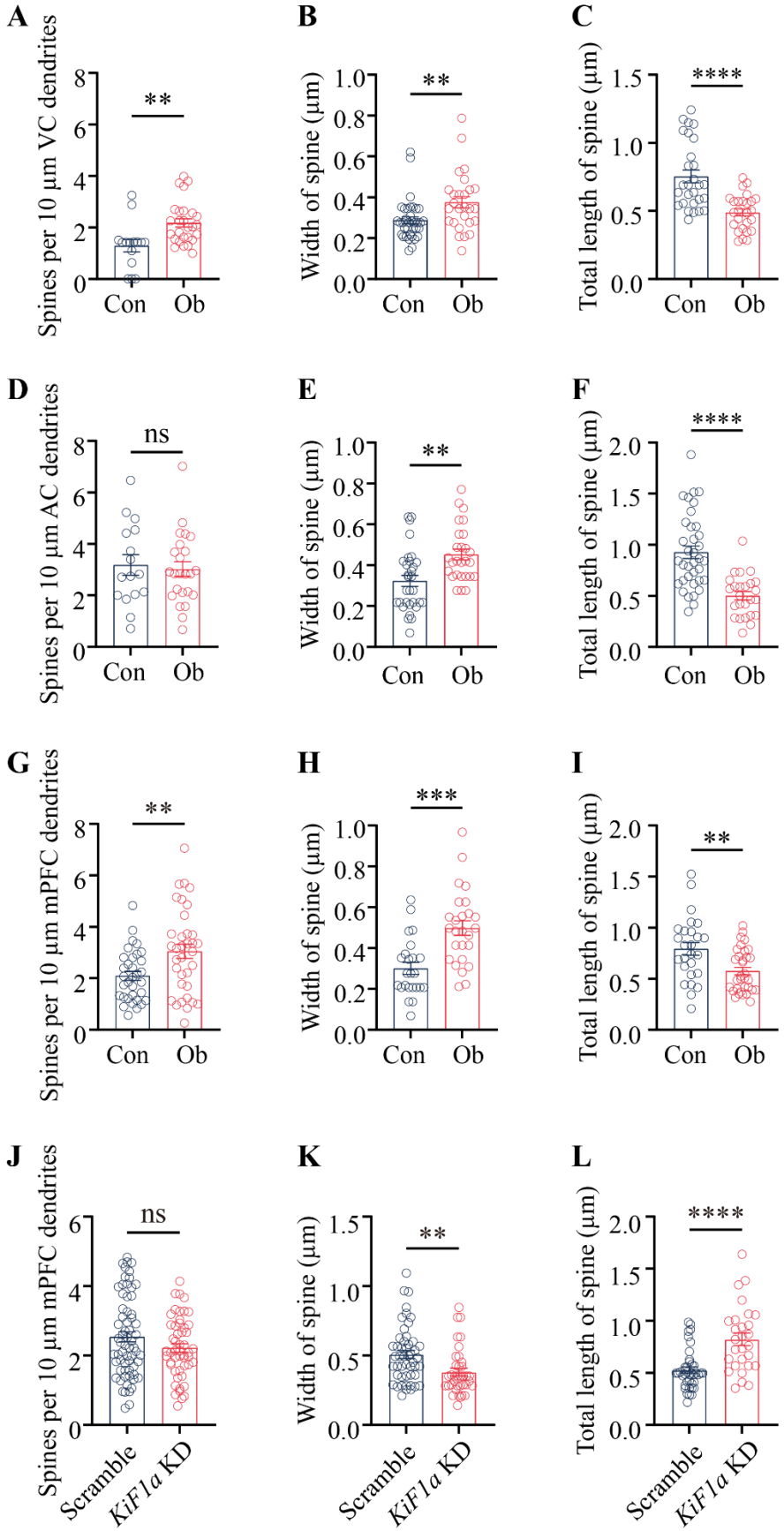

Extended Data Figure 5: Spine morphology changes in control, Ob, scramble, and *KiF1a*

RNAi groups. A) Statistic on the number of spines in VC of Con and Ob mice. **B)** Statistic on the width of spine in VC of Con and Ob mice. **C)** Statistic on the total length of spine in VC of Con and Ob mice. **D)** Statistic on the number of spines in AC of Con and Ob mice. **E)** Statistic on the width of spine in AC of Con and Ob mice. **F)** Statistic on the total length of spine in AC of Con and Ob mice. **G)** Statistic on the number of spines in mPFC of Con and Ob. **H)** Statistic on the width of spine in mPFC of Con and Ob mice. **I)** Statistic on the total length of spine in mPFC of Con and Ob mice. **J)** Statistic of the number on spines in mPFC of scramble and *KiF1a* KD mice. **K)** Statistic on the width of spine in mPFC of scramble and *KiF1a* KD mice. **L)** Statistic on the length of spine in mPFC of scramble and *KiF1a* KD mice. Abbreviations: Con: control; Ob: observer; VC: visual cortex; AC: auditory cortex; KD: knock down. Data are shown as mean ± SEM and analyzed by one-way ANOVA. Four asterisks, $p < 0.0001$; three asterisks, $p < 0.001$; two asterisks, $p < 0.01$; ns, $p > 0.05$.